NASA Technical Memorandum 78,465

(NASA-TM-78465) PHASE RELATIONS IN THE Fe-Ni-Cr-S SYSTEM AND THE SULFIDATION OF AN AUSTENITIC STAINLESS STEEL (NASA) 55 p HC A04/MF A01 CSCL 11F
N78-17147
Unclas
G3/23 04455

Phase Relations in the Fe-Ni-Cr-S System and the Sulfidation of an Austinitic Stainless Steel

K. T. Jacob, D. Bhogeswara Rao,
and Howard G. Nelson

December 1977

FEB 1978
RECEIVED
NASA STI FACILITY

National Aeronautics and
Space Administration

Ames Research Center
Moffett Field, California 94035

Phase Relations in the Fe-Ni-Cr-S System and the Sulfidation of an Austinitic Stainless Steel

K. T. Jacob,* D. Bhogeswara Rao,† and Howard G. Nelson‡

---

*Department of Mechanical Engineering, University of California, Berkeley, California 94720. (Visiting scientist from Department of Metallurgy and Materials Science, University of Toronto, Canada.)

†Materials and Molecular Research Division, Lawrence Berkeley Laboratory, Berkeley, California 94720, and Materials and Physical Science Branch, Ames Research Center, NASA, Moffett Field, California 94035.

‡Materials and Physical Science Branch, Ames Research Center, NASA, Moffett Field, California 94035.

ABSTRACT

The stability fields of various sulfide phases that form on Fe-Cr, Fe-Ni, Ni-Cr and Fe-Cr-Ni alloys have been developed as a function of temperature and the partial pressure of sulfur. The calculated stability fields in the ternary A-B-S system are displayed on plots of log P_{S_2} versus the conjugate extensive variable (n_A/n_A+n_B), which provides a better framework for following the sulfidation of Fe-Cr-Ni alloys at high temperatures. Experimental and estimated thermodynamic data were used in developing the sulfur potential diagrams. Current models and correlations were employed to estimate the unknown thermodynamic behavior of solid solutions of sulfides and to supplement the incomplete phase diagram data of geophysical literature. These constructed stability field diagrams are in excellent agreement with the sulfide phases and compositions determined experimentally during the sulfidation of SAE 310 stainless steel. The sulfur potential plots appear to be very useful in predicting and correlating the sulfidation of commercial alloys.

INTRODUCTION

The results on the sulfidation of SAE 310 stainless steel as a function of sulfur potential at a temperature of 1065 K[1] and as a function of temperature at three different sulfur potentials,[2] have been reported earlier. Generally, the sulfide scales are multilayered, containing one or two outer layers in addition to a subscale. The number of scales and their composition varied with the sulfur potential and the temperature of sulfidation. In two layered scales, the second outer layer (OL-II), furthest from the alloy, contained primarily phases of the Fe-Ni-S system. The first outer layer (OL-I), nearest the subscale, contained phases of the Fe-Cr-S system. The subscale consisted of chromium rich sulfide inclusions in the alloy matrix. The chromium content of OL-I increased with increasing temperature and decreasing sulfur potential, and appeared to control the rate of sulfidation of 310 stainless steel. However, correlations between the compositions of the experimentally observed phases and those that may be theoretically predicted have not been explored.

The purpose of this paper is to present the thermodynamic stability fields for sulfide phases in the ternary systems of Fe-Cr-S, Fe-Ni-S and Ni-Cr-S and in the quarternary system of Fe-Cr-Ni-S calculated using current models and correlations to compensate for incomplete thermodynamic data. The calculated stability fields are, then, compared with sulfide phases and compositions obtained experimentally following the dynamic sulfidation of SAE 310 stainless steel.

REPRESENTATION OF PHASE EQUILIBRIA

Phase diagrams are geometric representations of the loci of thermodynamic parameters when equilibrium between different phases exists under a specified set of conditions. Since there are many parameters such as temperature composition, pressure, chemical potential, etc., which may be used to define the axes of a diagram, many different kinds of phase diagrams can be constructed. To better understand the corrosion behavior of three or four component systems, a plot of the logarithm of the partial pressure of the nonmetallic component versus the mole fraction of the metallic components at a constant temperature is advantageous. A diagram of this type is shown in Fig. 1 for a three component system. In the case of a four component system containing a volatile, nonmetallic element, the compositions of the three metallic components are represented at a constant temperature on a Gibb's triangle and the logarithm of the partial pressure of the volatile element is plotted along an axis perpendicular to the plane of the Gibb's triangle. The advantage of this type of presentation is that it can readily be interpreted by anyone familiar with the topological rules for the construction of the well known temperature-composition diagrams for binary systems. The use of the mole fraction of the metal component on the abscissa allows one to use the familiar lever principle to graphically assess the relative quantities of each phase present in two phase regions. It can be shown by rigorous thermodynamic analysis that all of the other construction rules for the usual binary temperature-composition diagrams are applicable to this type of construction. For example, lines do not cross and intersecting phase boundaries obey certain angular relationships known sometimes as the extension rules.

EARLIER WORK ON PHASE RELATIONS

Extensive information is available in geophysical literature on phase relations in the Fe-Ni-S system.[3-13] Two isothermal Gibb's triangles representing the phase relations of Fe-Cr-S system at 873 K and 973 K are also available.[14,15] No information exists on the Ni-Cr-S ternary and Fe-Cr-Ni-S quarternary systems. Most available information relates to the structure and composition of the phases present in samples after equilibrating in evacuated silica capsules at specific temperatures. Unfortunately, the sulfur potentials in equilibrium with the various phases or phase mixtures have not been measured. This gap makes it difficult to predict the structure and composition of the phases that will form during sulfidation experiments, where the temperature and sulfur potential are carefully controlled. It is necessary, therefore, to combine experimental and estimated thermodynamic values with information on phase relations, to calculate the sulfur potentials associated with single and multiphase equilibria. The selection of the basic data and the models and correlations used to estimate the unknown thermodynamic data are described below.

BINARY DATA

Fe-S System

The phase diagram of the Fe-S system reveals the formation of two compounds FeS and FeS_2 in addition to Fe - FeS eutectic.[16] FeS has a wide range of nonstoichiometry and melts over a temperature interval of 100° and dissociates into a sold richer in sulfur and a liquid richer in iron until the approximate composition $Fe_{0.92}S$ is reached. This compound melts

congruently at 1463 K under the pressure of the system. The standard free energy of formation of $Fe_{1-x}S$ is well established.[17-20] For the reaction

$$Fe(s) + 1/2S_2(g) \rightarrow Fe_{1-x}S(s) \quad (1)$$

the standard free energy of formation can be expressed as

$$\Delta G^\circ = -151,500 + 54.1T\ (\pm 1,500)\ J\ mole^{-1} \quad (2)$$

FeS_2 can exist in one of two forms (marcasite at low temperatures and pyrite at high temperatures) with a transformation temperature of about 635 K. FeS_2 decomposes around 980 K yielding mono-sulfide and elemental sulfur. The standard free energy for the reaction

$$Fe(s) + S_2(g) \rightarrow FeS_2(s) \quad (3)$$

can be represented[21] as

$$\Delta G^\circ = -334,700 + 240.5T\ (\pm 800)\ J\ mole^{-1} \quad (4)$$

The sulfur potential corresponding to the two phase equilibrium between $Fe_{1-x}S$ and FeS_2 is given by the relation

$$\Delta\mu_{S_2} = -363,700 + 375T\ (\pm 1,000)\ J\ mole^{-1} \quad (5)$$

Pure iron melts at a temperature of 1810 K and the eutectic in the system Fe - FeS is at a temperature of 1260 K.

Cr-S System

In the binary Cr-S system, Jellinek[22] has suggested the existence of six definite chromium sulfides at room temperature: CrS (monoclinic), Cr_7S_8, Cr_5S_6, Cr_3S_4, Cr_2S_3 (triclinic) and Cr_2S_3 (rhombohedral) with superstructures of the NiAs type. At temperatures around 973 K, El Goresy and Kullerud[14,15] have shown that only two stable phases exist; $Cr_{1-x}S$ with a homogeneity range

between 51.8 and 55.5 at pct S and Cr_2S_3 with a homogeneity range between 57.1 and 58.8 at pct S. The $Cr_{1-x}S$ phase crystallizes in two types of structures depending on composition. Between 51.8 and 53.8 at pct S a NiAs type hexagonal form is observed and between 54.05 and 55.6 at pct S a hexagonal form with NiAs supercell is obtained. These findings have been substantiated by recent studies of Popma and van Bruggen[23] using high temperature X-ray diffraction, differential thermal analysis and magnetic methods. El Gorsey and Kullerud[14,15] have pointed out that the X-ray diffraction pattern given by Jellinek[22] for Cr_3S_4 is identical with that of composite reflections produced from a mixture of monoclinic $Cr_{1-x}S$, which forms at low temperatures, and rhombohedral Cr_2S_3. Ordering of vacancies at low temperatures breaks up the high temperature single phase field of $Cr_{1-x}S$ into a number of structures with compositions close to $Cr_{0.96}S$, Cr_7S_8, and Cr_5S_6.

The H_2S/H_2 ratios in the gas phase required for the initiation of sulfidation of pure metallic chromium between 1375 K and 1570 K have been measured by Hager and Elliott.[24] Young, et al.[25] measured a variation of the equilibrium H_2S/H_2 ratio with composition in the Cr-S system at 973 K. The standard free energy of formation of the metal saturated $Cr_{1-x}S$ phase at 973 K obtained from these two gas equilibration studies are compared in Table 1 with values obtained from an analysis of phase relations in the Fe-Cr-S system (see Fe-Cr-S ternary).

It is evident from Table 1 that disagreement exists between the values for free energy of formation of $Cr_{1-x}S$ obtained by gas equilibrium techniques and those derived from the phase diagram. It is likely that oxygen contamination of the sulfide phase during the gas equilibrium studies may have occurred and increased the stability of the $Cr_{1-x}S$ phase. Hager and Elliott[24] did not unequivocally characterize the sulfide phase formed in their

experiments, while Young, et al.[25] interpreted their results in terms of the phases reported by Jellinek[22] at room temperature. In the phase diagram studies of El Goresy and Kullerud[14,15] some contamination of the Fe+Cr alloy by silicon may have occurred, since the alloy was contained in evacuated silica capsules. Small amounts of dissolved silicon, however, will not drastically change the composition of the conjugate phases. The selected value for the free energy of formation $Cr_{1-x}S$ is, therefore, weighted in favor of the phase equilibrium studies. For the reaction

$$Cr(s) + 1/2S_2(g) \rightarrow Cr_{1-x}S(s) \tag{6}$$

the free energy change can be represented as

$$\Delta G^\circ = -192{,}000 + 60.7T\ (\pm 10{,}000)\ J\ mole^{-1} \tag{7}$$

The heat of formation of solid Cr_2S_3 from metallic chromium, iron and rhombohedral sulfur at 298 K is given in the literature as -347 kJ $mole^{-1}$. The entropy of formation of Cr_2S_3 according to the reaction,

$$2Cr(s) + 3/2S_2(g) \rightarrow Cr_2S_3(s) \tag{8}$$

is estimated as 188 J $mole^{-1}K^{-1}$. Therefore, free energy change for the reaction (8) can be expressed as

$$\Delta G^\circ = -527{,}200 + 188T\ (\pm 5{,}000)\ J\ mole^{-1} \tag{9}$$

The heat capacities of the sulfide phases used in the above evaluation are based on the methods described by Mills[21] and Kubaschewski, et al.[26]

The sulfur potential corresponding to the equilibrium between $Cr_{1-x}S$ and Cr_2S_3 is estimated as,

$$\Delta\mu_{S_2} = -26[illegible],00 + 121T\ (\pm 5{,}000)\ J\ mole^{-1} \tag{10}$$

based on the results of Young et al.[25] at 973 K and Igaki et al.[27] between 1200 K and 1400 K. The recent results of Nishida et al.[28] are inconsistent with the selected values and the sulfur potentials calculated from these data are orders of magnitude higher than the others.

Ni-S System

The most recent phase diagram of the Ni-S system is given by Craig and Scott.[29] Numerous measurements of the thermodynamic data on the binary Ni-S system are reported in the literature,[19,30-36] and the data are in mutual agreement. The values used in the present work are those obtained by Meyer et al.,[31] between 1373 K and 1973 K and the information summarized by Mills[21] for the lower temperatures, supplemented by recent data of Lin et al.[35] using gas equilibrium techniques, and Conrad et al.[36] using drop calorimetry.

TERNARY DATA

Fe-Cr-S System

$Fe_{1-x}S$ - $Cr_{1-x}S$ Solid Solution

The ternary phase relations at 973 K mapped by El Goresy and Kullerud[14,15] are shown in Fig. 2. There is an asymetric miscibility gap in the $Fe_{1-x}S$ - $Cr_{1-x}S$ pseudo binary and a stable ternary compound (iron sulfochromite ($FeCr_2S_4$)) with a spinel structure. This spinel phase is called daubreelite in geological literature. Since the formation of a monosulfide solid solution involves the mixing of Fe^{2+} and Cr^{2+} ions on the cation sublattice, the enthalpy and free energy of mixing can be evaluated from the miscibility gap using a subregular solution model[37] as

$$\Delta H^M = X_{CrS}X_{FeS}\{19{,}540\ X_{CrS} + 5{,}020\ X_{FeS}\}\ \text{J mole}^{-1} \quad (11)$$

$$\Delta G^M = \Delta H^M + RT\{X_{CrS}\ \ln X_{CrS} + X_{FeS}\ \ln X_{FeS}\}\ \text{J mole}^{-1} \quad (12)$$

$$\Delta G_{CrS} = RT\ \ln a_{CrS} = -34{,}100\ X_{FeS}^2 - 29{,}100\ X_{FeS}^3 + RT\ \ln X_{CrS}\ \text{J mole}^{-1} \quad (13)$$

$$\Delta G_{FeS} = RT\ \ln a_{FeS} = -9{,}520\ X_{CrS}^2 - 29{,}100\ X_{CrS}^3 + RT\ \ln X_{FeS}\ \text{J mole}^{-1} \quad (14)$$

On the basis of these equations, the critical temperature above which the miscibility gap vanishes is calculated to be 1070 K.

The tie lines in Fig. 2 between the alloy and the monosulfide solid solution represent exchange reactions of the type,

$$FeS(s) + Cr(s) \rightarrow CrS(s) + Fe(s) \quad (15)$$

for which the standard free energy change can be calculated as,

$$\Delta G^\circ = RT\ \ln \frac{a_{CrS} \cdot a_{Fe}}{a_{FeS} \cdot a_{Cr}} \quad (16)$$

$$\Delta G^\circ_{973\ K} = -13{,}000\ (\pm 2{,}000)\ \text{J mole}^{-1} \quad (17)$$

The values for the activities of CrS and FeS in the monosulfide phase can be obtained from Eqs. (13) and (14), while the activities of Fe and Cr in the alloy are given in the compiliation of Hultgren, et al.[38] Combining the Eqs. (2) and (17) one obtains the standard free energy of formation of $Cr_{1-x}S$ according to Eq. (6);

$$\Delta G^\circ_{973\ K} = -111{,}900\ (\pm 3{,}500)\ \text{J mole}^{-1} \quad (18)$$

The above calculation assumes that the compositions of the monosulfide phase in equilibrium with the alloy fall on a pseudo-binary join. A careful perusal of the phase diagram (Fig. 2) suggests that the sulfur concentration

of the monosulfide phase in equilibrium with the alloy varies with the Fe/Cr ratio. For an exact analysis, therefore, the free energy of formation of the monosulfide solid solution as a function of Fe/Cr ratio and sulfur concentration must be evaluated. This can be done by expressing the integral molar free energy of the monosulfide phase as a power series in mole fraction of sulfur for different Fe/Cr ratios. The values of the coefficients of the power series for pure $Fe_{1-x}S$ and $Cr_{1-x}S$ phases are evaluated from the corresponding binary data. The free energy surface for the solid solution can be generated by assuming that the coefficients in the power series vary linearly with composition between the two binary ends. The points of common tangency to the free energy surface for the alloy and sulfide phase are obtained by solving the three equations,

$$\Delta\mu_i^{\text{sulfide}} = \Delta\mu_i^{\text{alloy}} \quad (i = \text{Fe, Cr, S}) \tag{19}$$

A detailed analysis along these lines suggests that the standard free energy of formation of metal saturated $Cr_{1-x}S$ phase is -8 kJ $mole^{-1}$ more negative than the simple analysis outlined earlier. The value calculated in Eq. (18) is then modified to become -120 kJ $mole^{-1}$. The value used in this investigation was -130 (±10) kJ $mole^{-1}$ for the $\Delta G^{\circ}_{973\ K}$ and is a compromise (Table 1, and Eq. (7)).

$FeCr_2S_4$ (Iron Sulfochromite)

The heat of formation of iron sulfochromite, $FeCr_2S_4$, from iron, chromium and rhombohedral sulfur has been recently measured by Kessler, et al.[39] by combustion calorimetry as -457 (±8) kJ $mole^{-1}$ at 298 K. On the basis of this value the free energy of formation of $FeCr_2S_4$ from FeS and CrS at high temperatures may be evaluated;

$$FeS(s) + CrS(s) + 1/2S_2(g) \rightarrow FeCr_2S_4(s) \quad (20)$$

$$\Delta G^\circ = -177,800 + 71T\ (\pm 8,000)\ J\ mole^{-1} \quad (21)$$

Alternatively, the free energy of formation of $FeCr_2S_4$ can be expressed as,

$$FeS(s) + Cr_2S_3(s) \rightarrow FeCr_2S_4(s) \quad (22)$$

$$\Delta G^\circ = -27,200 + 4.2T\ J\ mole^{-1} \quad (23)$$

Vogel and Heumann,[40] and El Goresy and Kullerud[14,15] have documented evidence for four-phase equilibrium in the Fe-Cr-S system at 923 (±50) K, which can be represented by the equation,

$$3.68(Fe_{0.53}Cr_{0.47})_{1-x}S(s) + 0.32(Fe_{0.15}Cr_{0.85})_{1-x}S(s) \rightarrow Fe(s) + FeCr_2S_4(s) \quad (24)$$

The selected values for the free energy of formation of $Fe_{1-x}S$, $Cr_{1-x}S$ and $FeCr_2S_4$ and the free energy of mixing of $Fe_{1-x}S$ - $Cr_{1-x}S$ solid solution correctly predict the free energy change for the invariant reaction which must be zero at 923 K. This lends further credence to the correctness of the selected values.

Isothermal Plots of log P_{S_2} vs $(n_{Cr}/(n_{Cr} + n_{Fe}))$

Having evaluated the values for Gibb's free energies of various phases in the Fe-Cr-S system, it is possible to construct isothermal plots of log P_{S_2} versus the mole fraction of chromium $(n_{Cr}/(n_{Cr} + n_{Fe}))$. Two interrelated techniques are used in calculating the stability fields of the various phases.

In the first technique, an expression is developed for the total free energy of the system. Free energy is minimized with respect to the number of moles of each component in each phase, under the constraint that the total

number of moles of each component remain constant. Although, conceptually simple, the solution of these equations for various temperatures and partial pressures of sulfur is complex and numerical techniques are required. The detailed formulation of the numerical techniques have been given by Counsell, et al.[41] and Gaye and Lupis.[42] A simplified version of this technique is to plot the free energy as a function of composition along pseudo-binary section of the ternary system. The stability fields can then be evaluated by applying the principle that the stable phase or phase mixture has the lowest free energy (or the lowest common tangent on the free energy-composition diagram).

A corollary of the stability criterion in terms of the minimization of the free energy is that the chemical potential of each component in conjugate phases must be equal. This equality, expressed by Eq. (19), can be used to calculate the compositions of the conjugate phases. Because of the transcendental nature of Eq. (19), its solution requires, except in the simplest cases, the use of numerical techniques. The least sophisticated of these is the Gauss-Seidel technique.[43] For a ternary system, three simultaneous equations must be solved for calculating the composition of the conjugate phases. The number of steps used in the computation depends on the accuracy of the thermodynamic data. For the Fe-Cr-S system uncertainties in the data do not justify more than five steps. This method is only capable of calculating the compositions along two-phase boundaries, and other considerations must be brought to bear in coordinating the various phase fields in the final diagram. Alternatively, for any chosen value of temperature and sulfur potential, one starts with a given composition of the alloy phase, and by solving Eq. (16) one obtains a value for the composition $(n_{Cr}/(n_{Cr} + n_{Fe}))$ of the monosulfide phase in equilibrium with the alloy.

The sulfur potential corresponding to the three-phase equilibria can readily be calculated as a function of temperature, if the free energies of the three phases and their compositions are known. The calculation is straightforward, if the phases in equilibrium are of stoichiometric composition. If solid solutions of varying composition are involved, the composition of the phases must be evaluated at each temperature and sulfur potential by first calculating the two phase boundaries and then projecting their extensions into the three-phase field.

In general for ternary and quarternary systems in which some experimental data is available, there is no general formula for approximating the missing data and for calculating the phase diagram. In such cases, one must use what is available and apply a measure of experience and judgment in making approximations and choosing numerical techniques for computation.

Figure 1 shows the various phase fields in the Fe-Cr-S system at 1275 K. The estimated uncertainties in the computed compositions and partial pressures of sulfur are indicated near the center of the figure. The diagram can broadly be divided into two regions; a lower region containing the two phase fields in which alloy is in equilibrium with the monosulfide solid solution and an upper region involving the spinal phase ($FeCr_2S_4$) in equilibrium with either $(Fe,Cr)_{1-x}S$ or Cr_2S_3. A continuous range of monosulfide solid solution exists. When the sulfur pressure over the system is increased above atmospheric pressure, a point is reached where liquid sulfur condenses as a separate phase. Although the condensation pressure of sulfur would vary slightly with iron or chromium concentration of the sample, because of differing solubility of the various sulfide phases in the liquid, such variations are not significant enough to be visible on the diagram. Strictly

the sulfur pressure over the Fe-Cr-S system cannot be increased monotonically above the condensation pressure, and the vertical axis should terminate at this point. However, one may explore metastable equilibria at higher sulfur pressures by suppressing the condensation process. Such metastable extensions are indicated by the dotted lines and are useful for locating the boundaries of the various phase fields. The metastable extensions obey the same topographical rules of construction.

Figures 3 and 4 show similar plots of log P_{S_2} versus $(n_{Cr}/(n_{Cr} + n_{Fe}))$ for 1065 K and 900 K, respectively. It is clearly evident from these plots that the gap between the upper and lower regions gradually decreases upon lowering the temperature. At 900 K (Fig. 4) the two regions have merged, thus breaking the continuity of the monosulfide single phase field. As it will be discussed in a later section, the sulfidation path of any Fe-Cr alloy can be followed on these diagrams and the composition of the phases that form at different sulfur potentials can be evaluated. The effect of temperature on the various phase fields at a constant partial pressure of sulfur ($P_{S_2} = 10^{-1}$ Nm^{-2} or 10^{-7} atm) is shown in Fig. 5.

Fe-Ni-S System

There are three condensed phases in the Fe-Ni-S system, bravoite ($(Fe,Ni)S_2$), violorite (Ni_2FeS_4) and pentlandite ($(Fe,Ni)_9S_8$) in addition to the continuous range of solid solubility between $Fe_{1-x}S$ and $Ni_{1-x}S$ and the extended range of solubility between the liquid sulfides. Of these phases, bravoite and violorite are not stable at high temperatures and sulfur potentials of interest in coal conversion systems.

$Fe_{1-x}S$ - $Ni_{1-x}S$ Solid Solution

The free energy of mixing of the $Fe_{1-x}S$ - $Ni_{1-x}S$ monosulfide solid solution, estimated from the difference in ionic radii of Fe^{2+} and Ni^{2+}, can be represented as

$$\Delta G^M = 3{,}600\ X_{FeS}\ X_{NiS} + RT\ (X_{FeS}\ \ln X_{FeS} + X_{NiS}\ \ln X_{NiS})\ J\ mole^{-1} \quad (25)$$

The free energy of mixing of liquid sulfides is close to ideal values at a constant mole fraction of sulfur.

$FeNiS_{1.68}$ (Pentlandite)

Kullerud[4] has shown from quenching experiments, differential thermal analysis, and high temperature X-ray diffraction that synthetic pentlandite of composition $FeNiS_{1.68}$ decomposes at 883 (±2) K in the presence of sulfur vapor into an iron rich monosulfide solid solution and a high temperature non-quenchable phase, $Ni_{3-x}S_2$. Studies of Shewman and Clark[8] confirm the decomposition of pentlandite, but show that the iron and nickel solid solubility limits are greater than those shown by Kullerud.[4] Recently Conrad, et al.[36] have redetermined the decomposition temperature, as 890 (±2) K, using differential thermal analysis. They have also measured the heat capacity of pentlandite from 400 K to 1400 K by dropping samples equilibrated at high temperatures into a room temperature calorimeter. There is a discontinuity in heat capacity which is attributed to the decomposition of pentlandite,

$$3FeNiS_{1.68}(s) \rightarrow 3FeS(s) + Ni_3S_2(s) \quad (26)$$

The heat of dissociation deduced from these measurements is 12.78 kJ per mole of $FeNiS_{1.68}(s)$. Examination of the samples dropped from above 890 K

indicated the presence of (Fe,Ni)S phase. Conrad, et al.[36] did not correct their results for the presence of this quenched high temperature phase. Conrad, et al.[36] also reported the heat of formation of pentlandite obtained by acid solution calorimetry as -274 kJ $mole^{-1}$ for $FeNiS_{1.68}(s)$ at 890 K. When this value is combined with the heat of formation of Ni_3S_2 (Ref. 36) (-267.2 kJ $mole^{-1}$) and FeS (Ref. 25) (-142.7 kJ $mole^{-1}$) at 890 K, one obtains a value for the heat of dissociation of pentlandite as 42.2 kJ per mole of $FeNiS_{1.68}(s)$. This value is significantly different from that deduced from the heat capacity measurements. For the calculations of the present study we have accepted the value obtained from the heat capacity measurements in preference to that obtained from acid solution calorimetry.

If the decomposition of pentlandite is represented as a complete solid state process (Eq. (26)), then the entropy change would be 14.36 J per mole of $FeNiS_{1.68}(s)$ per degree at 890 K (Ref. 36). This large positive value for entropy is rather difficult to understand in view of the configurational gain in entropy of pentlandite due to the mixing of cations. It suggests, therefore, that gaseous diatomic sulfur is probably a product of decomposition. It is, therefore, proposed that the decomposition of pentlandite occurs according to the scheme,

$$Fe_{4.5}Ni_{4.5}S_8(s) \rightarrow 1.55(Ni_{0.95}Fe_{0.05})S_{1.99}(s) + 4.37(Fe_{0.98}Ni_{0.02})S_{1.02}(s) + 0.229S_2(g) \quad (27)$$

for which the standard free energy change is given by

$$\Delta G^\circ = 60{,}700 - 30T\ (\pm 3{,}000)\ J\ mole^{-1} \quad (28)$$

The partial pressure of diatomic sulfur corresponding to the decomposition at 890 K is 1.95×10^{-4} Nm^{-2} or 1.9×10^{-9} atm. It may appear that the reaction will not proceed to any significant extent in a closed system of small capacity, because the sulfur pressure would soon build up to the equilibrium value. The other two condensed phases present, however, have appreciable nonstoichiometry and can dissolve gaseous sulfur in their lattice. The reaction will proceed to completion over a limited range of sulfur pressure and temperature. The decomposition scheme given in Eq. (27) is also compatible with the measured pressure dependence of the decomposition temperature in the pressure range from 4×10^{7} Nm^{-2} to 3.6×10^{9} Nm^{-2} (Ref. 44).

Isothermal Plots of log P_{S_2} vs $(n_{Ni}/(n_{Ni} + n_{Fe}))$

Based on the thermodynamic data discussed above, plots of log P_{S_2} versus $(n_{Ni}/(n_{Ni} + n_{Fe}))$ at 1275 K, 1150 K and 900 K have been constructed and are shown in Figs. 6, 7 and 8, respectively. The methods used were analogous to those discussed for the Fe-Cr-S system. A two phase region must separate the single phase regions of α-(Fe,Ni) and $(Fe,Ni)S_{1-x}(l)$ in Fig. 6. Because the width of the alloy plus the two phase liquid sulfide field is narrow, it cannot be clearly shown in the figure. With increasing sulfur potential all alloys of the Fe-Ni system will first form a liquid (metal rich sulfide solution). The width of the liquid sulfide field is narrow for the iron rich alloys, and with increasing sulfur potential a monosulfide solid solution will result. At 1025 K there is no monosulfide phase field in the Ni-S binary. At the lower temperatures (1150 K and 900 K) there is a continuous range of monosulfide solid solutions, but the range of the sulfur deficient liquid sulfide field is progressively reduced with decreasing temperature

(Figs. 7 and 8). Finally, at 900 K (Fig. 8) there is no liquid sulfide phase, but a solid $Ni_{3+x}S_2$ phase with a wide range of homogeneity and a limited solubility for iron is present. At sulfur pressures close to one atmosphere both FeS_2 and NiS_2 phases are formed at 900 K with a limited range of solid solubility. The effect of temperature on the stability fields of the various phases at a fixed partial pressure of sulfur ($P_{S_2} = 10^{-2}$ Nm^{-2} or 10^{-7} atm) is shown in Fig. 9.

Ni-Cr-S System

The ternary Ni-Cr-S phase diagram is not available from the literature. The spinel compound $NiCr_2S_4$ has been identified, during the sulfidation of Ni-Cr alloys.[45] There is no thermodynamic data on either the spinel compound or the solid and liquid solutions in the Ni-Cr-S system. Since the ionic radii of Ni^{2+} and Cr^{2+} are 0.84 A and 0.87 A, respectively, on the Shannon Prewilt scale for sixfold coordination, mixing of these cations may be assumed to be ideal. It follows that activities in the liquid and monosulfide phases are equal to mole fractions at constant sulfur concentrations. In the $(Cr,Ni)_2S_3$ solid solution the activity of each component is equal to the square of the molefraction,

$$a_{Ni_2S_3} = X^2_{Ni_3S_2} \tag{29}$$

$$a_{CR_2S_3} = X^2_{Cr_2S_3} \tag{30}$$

since there are two cations in each molecule of the components in the mixture.

$NiCr_2S_4$ (Nickel Sulfochromite)

Recent studies[46-51] have shown certain regularities in the heats of formation of 2-3 spinels ($M^{2+}X_2^{3+}O_4$), from component oxides MO and X_2O_3. For example plots of the heats of formation of aluminates and chromites as a function of the group number of the divalent cation produces two sets of parallel curves thus indicating that the difference in the heats of formation of aluminate and chromite spinels are almost the same (±4,000 J $mole^{-1}$). The heat of formation of the iron sulfochromite ($FeCr_2S_4$) from its component sulfides FeS and Cr_2S_3 has been evaluated earlier as -27,200 J $mole^{-1}$ (Eq. (23)). This value is close to the heat of formation of $FeAl_2O_4$ which is -27,800 J $mole^{-1}$. The heats of formation of other sulfochromites can, therefore, be considered to be equal to those of the corresponding aluminates. The heat of formation of $NiCr_2S_4$ is estimated, accordingly, as

$$NiS(s) + Cr_2S_3(s) \rightarrow NiCr_2S_4(s) \tag{31}$$

$$\Delta H^\circ = -5{,}900 \text{ J mole}^{-1} \tag{32}$$

The entropy of formation of 2-3 spinels from their component binary compounds can be represented as,[48-51]

$$\Delta S = k + \Delta S^M + \Delta S^{JT}_{rand} \text{ J mole}^{-1} \tag{33}$$

where k is a constant having a value of -7.3 (±1.2) for oxide spinels, ΔS^M is the entropy of cation mixing in the tetrahedral and octahedral sites of the spinel structure, and ΔS^{JT} in the Jahn-Teller entropy associated with the randomization of the orientation of orbitals with prolate or oblate distortions. The value of ΔS^{JT} is 8.8 J $mole^{-1}K^{-1}$ and ΔS^M has a value of 2.3 J $mole^{-1}K^{-1}$ for $NiCr_2S_4$. The value of the constant k for the

2-3 sulfospinels can be evaluated as -4.3 J $mole^{-1}K^{-1}$ by comparing Eq. (33) with the value of the entropy of formation of $FeCr_2S_4$ evaluated earlier (Eq. (23)). The entropy of formation of $NiCr_2S_4$ according to Eq. (31) can, therefore, be estimated as 6.8 J $mole^{-1}K^{-1}$.

Isothermal Plot of Log P_{S_2} vs $(n_{Cr}/n_{Cr} + n_{Ni})$

The stability field diagram for Ni-Cr-S system has been constructed only at 1275 K and is shown in Fig. 10. This diagram is based on the estimated thermodynamic data on sulfides reviewed above and the information on binary Ni-Cr alloys summarized by Hultgren, et al.[38] An interesting feature of this diagram is the limited range of solubility between the chromium rich monosulfide phase and the nickel rich liquid sulfide phase. As will be seen, this particular information is very useful in interpreting the sulfidation behavior of SAE 310 stainless steel.

QUARTERNARY SYSTEM: Fe-Cr-Ni-S

In order to construct the Fe-Cr-Ni-S quarternary phase diagram the following information is required;

1. Free energy of mixing of the Fe-Ni-Cr alloy
2. Free energy of mixing of the pseudo-ternary monosulfide solid solution $(Fe,Ni,Cr)_{1-x}S$
3. Free energy of mixing of the sulfur deficient ternary liquid sulfide phase $(Fe,Ni,Cr)S_{1-x}(1)$
4. Activities in the $FeCr_2S_4$-$NiCr_2S_4$ spinel solid solutions

The first three sets of information regarding the free energy of mixing of ternary or pseudo-ternary systems can be expressed as a sum of contributions

of the corresponding binary systems at points that are closest to the ternary compositions.[52] For example this can be expressed as

$$\Delta G^{M,E}_{Fe,Ni,\ Cr} = X_{Fe}X_{Ni}\ \{B_o + B_1(X_{Fe} - X_{Ni}) + B_2(X_{Fe} - {}_{Ni})^2 + \ldots\}$$
$$+ X_{Ni}X_{Cr}\ \{B'_o + B'_1(X_{Ni} - X_{Cr}) + B'_2(X_{Ni} - X_{Cr})^2 + \ldots\}$$
$$+ X_{Cr}X_{Fe}\ \{B''_1(X_{Cr} - X_{Fe}) + B''_2(X_{Cr} - X_{Fe})^2 + \ldots\} \qquad (34)$$

where B_o, B_1, and B_2 are the empirical constants for the binary Fe-Ni system, B'_o, B'_1 and B'_2 correspond to the Ni-Cr system and B_o, B_1 and B_2 represent the data on the Cr-Fe alloys. These constants are obtained by expressing the binary values as a power series in $(X_i - X_j)$ (Ref. 52). The composition paths on the Ternary Gibb's triangle, along which $(X_i - X_j)$ are constant, correspond to perpendiculars drawn from any point inside the triangle to its sides.[52]

Activities in the spinel solid solution can be calculated using a complex model[53] that computes the configurational entropy gain due to the redistribution of three cations between the tetrahedral and octahedral sites governed by the site preference energies of the cations.[48] The heat of cation redistribution is also evaluated from the site preference energies.

The quarternary phase diagram at a fixed temperature can in principle be represented by plotting the logarithm of the partial pressure of sulfur on an axis perpendicular to the composition triangle on which the composition of the Fe-Ni-Cr alloys are located. The stability fields of the various phases are then located within the volume of the prism. The sides of the prism represent the ternary phase diagrams of the Fe-Cr-S, Fe-Ni-S, and Ni-Cr-S systems. The edges of the prism represent the influence of sulfur on the stability fields. The quarternary phase fields occupy the interior of the

prism. Since a space model of the type described is too complex for graphical display, an example is given in Fig. 11 of the sulfide phases and their compositions that would be expected to be formed at 1275 K on SAE 310 stainless steel at different sulfur potentials. For the purpose of this construction SAE 310 stainless steel is considered as an Fe-Ni-Cr alloy containing 54 at pct Fe, 20 at pct Ni and 26 at pct Cr. The presence of minor amounts of other elements Mn(1.7), Si(0.72), Mo(0.49), Co(0.38), Cu(0.21), C(0.05), P(0.035) and S(0.01) have been ignored. The activities in the idealized alloy are: $a_{Fe} = 0.55$, $a_{cr} = 0.34$, and $a_{Ni} = 0.15$. Five major phase fields are identified in Fig. 11. The actual compositions of the sulfide solid solutions, which change with the sulfur potential, are shown at regular intervals of sulfur potential. All the phases in a quarternary diagram can indeed be extrapolated from a study of the three ternary systems. For this reason the time consuming calculation of the quarternary phase fields have been attempted only at one temperature.

MECHANISM OF SULFIDATION OF ALLOYS

It can be highly instructive to follow the progress of sulfidation of alloys on the basis of stability field diagrams. For this purpose an alloy has been chosen having a Fe/Cr ratio the same as in SAE 310 stainless steel (molefraction of Cr, $n_{Cr}/Cn_{Cr} + n_{Fe}) = 0.35$). The phase fields of the Fe-Cr-S system at 1275 K are displayed in Fig. 1. From this diagram it is seen that sulfidation of this alloy will occur at sulfur pressures in excess of $10^{-3.6}$ Nm^{-2}. At lower partial pressures of sulfur there will be some limited solid solubility of sulfur in the alloy. At P_{S_2} equal to $10^{-3.6}$ Nm^{-2},

the initial sulfide phase that forms is rich in chromium $(Cr_{0.96}Fe_{0.04})_{1-x}S$ as can be seen from Fig. 1 by drawing a horizontal line through the two phase lens (α + $(Cr,Fe)_{1-x}S$). As the sulfur pressure in the gas is increased, the alloy will become depleted in chromium and its composition will follow the lower curve to the iron-rich corner. Composition of sulfide phase will under equilibrium conditions follow the upper curve and also move towards the iron-rich corner. At any given sulfur pressure the composition of the alloy and the sulfide is given by the intersection of the horizontal tie line with the curves delineating the two phase region. When a sulfur pressure of 10^{-2} Nm^{-2} is reached, the Cr/Fe ratio of the sulfide phase is the same as that of the bulk alloy. The alloy phase in equilibrium with this sulfide contains approximately 1 at pct Cr. The monosulfide phase cannot contain more iron than the bulk alloy.

On increasing the sulfur pressure, no further change in sulfide composition will occur until a sulfur pressure of $10^{1.9}$ Nm^{-2} is reached. At this pressure the spinel phase, $FeCr_2S_4$, will form in the scale in addition to the monosulfide solid solution. The relative amount of spinel phase will gradually increase with increasing sulfur pressure. When a pressure of $10^{6.8}$ Nm^{-2} is reached, liquid sulfur will condense as an additional phase.

COMPARISON WITH EXPERIMENT

The validity of the sulfur potential diagrams can be evaluated by comparing the data with the experimentally observed results. The experimental data acquired on the sulfidation of SAE 310 stainless steel[1,2] permit such comparison. The calculated sulfur potential diagrams and the sulfidation tests were performed at identical temperatures and sulfur potentials thus

facilitating a direct comparison. There is, however, a difference between the real equilibrium data and a dynamic corrosion test. The sulfur potential diagrams describe the relationship between true equilibrium phases which are expected to form when a controlled stream of reactive gas mixture is percolated through a fine powder of the alloy. Such tests would be of little value in industrial corrosion tests. During a dynamic corrosion test, true equilibrium will occur only at the gas/scale interface, while the main reaction is probably controlled by a diffusion process. Consequently, the scales that develop during a dynamic corrosion test may exhibit morphologies that differ from those of the equilibrium phases.

The dynamic sulfidation of SAE 310 stainless steel has been studied over the temperature range from 910 K to 1285 K at sulfur potentials from 39 Nm^{-2} to 1.5×10^{-4} Nm^{-2} (Refs. 1, 2). All sulfide scales contained one or two surface layers in addition to a subscale. The second outer layer (OL-II), furthest from the alloy, contained primarily Fe-Ni-S. The first outer layer (OL-I), nearest to the subscale, contained Fe-Cr-S. The reaction was found to obey the parabolic rate law after an initial transient kinetic behavior.

Transient Kinetic Behavior

When the sulfide scales are adherent, their growth most often occurs at the alloy-scale interface and is accompanied by the outward diffusion of cations through the scale. Since the initial sulfide formed at the alloy-scale interface is rich in chromium and the scale formed at the later periods contain progressively less chromium, diffusion rates through the scale most probably vary with time, and results in "transient kinetic behavior." Once the composition of the corrosion product becomes constant, the scales tend

to grow at a steady rate. This "transient kinetic behavior" as well as the gradient in iron and chromium across the sulfide layer (OL-I) on SAE 310 stainless steel have been demonstrated by Rao and Nelson.[1]

Another interesting factor worth noting is the nonequilibrium widening of the two phase lens. Because of the presence of a diffusion gradient across the scale, the activities of the metal components at the scale-gas interface are always less than that at the alloy-scale interface. This causes the two phase lens in the phase diagram to be slightly wider for nonequilibrium sulfidation. The extent of this widening can only be evaluated when diffusion coefficients of the cations are available. In this respect, it may be noted that the diffusion rates in the sulfides are much greater than those of the oxides and, hence, the oxides may show greater nonequilibrium widening.

Comparison with OL-I (Fe-Cr-S System)

The compositions of the individual layers of a composite scale formed during the sulfidation of SAE 310 stainless steel have been carefully analyzed as function of temperature and sulfur potential and compared with what has been predicted by the sulfur potential diagrams. As already mentioned, the outer layer nearest the alloy (OL-I), formed during the corrosion tests, contained phases that belong primarily to Fe-Cr-S system.

The open circles in Fig. 1 show the sulfur potentials at which the sulfidation of SAE 310 stainless steel was investigated.[2] The experimentally determined composition of OL-I is shown by asterisks in the figure. Despite the fact that the presence of nickel has been ignored, the measured compositions are close to those predicted on the basis of the Fe-Cr-S ternary diagram. This is very encouraging, especially when the uncertainties in the

construction of nonequilibrium widening of the two phase field are taken into consideration. At the lowest sulfur pressure investigated[2] only a slight sulfidation of chromium is expected and at the two higher sulfur pressures complete sulfidation of chromium and iron should occur. The parabolic rate constant at the lowest sulfur pressure should, therefore, be significantly lower, as confirmed by experiment.[2]

At 1065 K (Fig. 3) the pattern of sulfidation of Fe-Cr alloy should be similar to that at 1275 K. The three experimental sulfur pressures lie in either the monosulfide phase field or monosulfide plus spinel phase field. Both iron and chromium should undergo sulfidation. The diagram indicates that the Fe/Cr ratio of the sulfide phase should be the same as that of the bulk alloy. This is again verified by the experiment,[2] and shown by the asterisks in Fig. 3.

At 900 K (Fig. 4), because of the discontinuity of the monosulfide solid solution phase field, the sulfidation behavior of the Fe-Cr alloy should be different from that at the higher temperatures. At the start of sulfidation, the chromium rich monosulfide phase will form. However, the maximum solubility of $Fe_{1-x}S$ in $Cr_{1-x}S$ of 13 mole pct is attained at $P_{S_2} = 10^{-8.3}$ Nm^{-2}.

Most of the chromium at the alloy interface is converted with the formation of a chromium rich monosulfide. On increasing the sulfur pressure, the monosulfide solid solution will react with the iron in the alloy to form the sulfospinel ($FeCr_2S_4$). Since the alloy is physically removed from the scale-gas interface, the amount of spinel formed will be limited by the outward diffusion of Fe^{2+} ions. Increasing the sulfur pressure above $10^{-3.7}$ Nm^{-2} would convert the chromium rich monosulfide phase into a mixture containing Cr_2S_3 and smaller amounts of $FeCr_2S_4$. The formation of a thin

layer of $FeCr_2S_4$ at the lower temperatures has been, in fact, detected experimentally.[2] Figure 12 shows the composition analysis of the scale developed on SAE 310 stainless steel at 933 K.

The effect of temperature on the phase fields of the Fe-Cr-S system at a sulfur partial pressure of 10^{-2} Nm^{-2} is shown in Fig. 5. Decreasing temperature is seen to increase the stability field of $FeCr_2S_4$. Since the diagram is determined under the constraint that $P_{S_2} = 10^{-2}$ Nm^{-2}, it does not give a quantitative picture of phase changes that occur during cooling of the corroded specimen. Despite this limitation, the tendency for the spinel to form at lower temperatures is supported by the observation that after slow cooling the microstructure of OL-I contains layered structures of Fe-Cr-S which differed in the Fe:Cr ratio. When the corroded specimen is given a rapid quench, only the monosulfide phase is observed.[2]

In the ternary Fe-Cr-Ni alloys, in which the Fe/Cr ratio and the Fe/Ni ratio are the same as in SAE 310 stainless steel, the initial sulfidation of Cr and Fe proceeds in a fashion similar to that of the binary Fe-Cr alloy with only minor changes in the sulfur potential and the composition of the phases due to altered activities in the ternary alloy (compare Figs. 1 and 11).

Comparison with OL-II (Fe-Ni-S System)

The initial sulfidation of chromium and iron causes the depletion of these elements and the enrichment of nickel at the alloy-scale interface. The nickel ions diffuse out through the scale. When P_{S_2} in the gas phase is above $10^{-1.65}$ Nm^{-2} and the temperature is in the range of 1275 K, a liquid Fe-Ni-S melt is formed (Fig. 6). This melt is rich in metallic components and deficient in sulfur. This phase will be immiscible with the underlaying

Fe-Cr-S layer of OL-I and initiates the development of the OL-II layer, the sulfide layer furthest from the alloy. At 1275 K the stability of the liquid phase is narrow, and when P_{S_2} is greater than $10^{-1.27}$ Nm^{-2}, the liquid phase will transform into a solid $(Fe,Ni)_{1-x}S$ solution (Fig. 6). This microstructure is shown in Fig. 13 where the growth of $(Fe,Ni)_{1-x}S$ solid phase from the liquid melt is evident. In the equilibrium quarternary diagram at 1275 K there is a continuous range of solid solution between the monosulfides of iron, chromium and nickel, although at the lower temperatures a miscibility gap develops between $(Fe,Cr)_{1-x}S$ and $(Fe,Ni)_{1-x}S$ or $(Fe,Ni)_{3\pm x}S_2$ solid solutions. Despite the presence of a continuous solid solution field, the $(Fe,Cr)_{1-x}S$ solid solution formed initially (OL-I) and the $(Fe,Ni)_{1-x}S$ (OL-II) that forms from the melt are in contact only along a single surface, and remain as separate phases during the sulfidation process. The interface between the two monosulfide phases should remain fairly sharp even after prolonged periods at high temperature. This is due to the conversion of diffusing chromium ions through the OL-I to the sulfide phase by displacement reaction with $Fe_{1-x}S$ (Eq. 5) and $Ni_{1-x}S$. On increasing the sulfur pressure above $10^{1.95}$ Nm^{-2}, the $FeCr_2S_4$ phase will appear as a corrosion product, with some $NiCr_2S_4$ dissolved in it (Fig. 6). The amount of $NiCr_2S_4$ in the spinel solid solution will increase with increasing sulfur pressure facilitating higher diffusion rates at higher sulfur potentials. The relative thickness of OL-II will increase with increasing sulfur potential which has been observed experimentally.[1]

In the sulfidation studies conducted at the highest sulfur potential (39 Nm^{-2}), it is expected on the basis of the quarternary diagram that Cr,Fe, and Ni will be completely corroded at 1275 K. The corrosion rates are

limited by the rate of transport of cations through the scale. At the intermediate sulfur potential (1.4×10^{-2} Nm^{-2}) complete corrosion of Cr and Fe is expected while Ni will not form sulfides (Fig. 6). At the lowest sulfur potential (1.5×10^{-4} Nm^{-2}) only superficial sulfidation of chromium is expected. The parabolic rate constants for sulfidation at 1275 K should decrease sharply with decreasing sulfur potential as observed experimentally.[2] At the intermediate sulfur pressure (1.4×10^{-2} Nm^{-2}) OL-II should become fully liquid at 1165 K (Fig. 9). Rao and Nelson[2] observed a liquid phase to drip from their specimen at 1145 K — in good agreement with the phase diagram.

Effect of Cooling

An important point that emerges from the discussion of the corrosion behavior of SAE 310 stainless steel at 1275 K is that the sequence of events can readily be predicted from the consideration of the three binary systems, Fe-Cr-S, Fe-Ni-S and Ni-Cr-S, with only minor changes in the sulfur pressures and compositions of the phase boundaries. The only major observation that needs further clarification is the microstructure of the Fe-Ni-S layer (OL-II), which was found to be composed of a mixture of $(Fe,Ni)_{1-x}S$ monosulfide solid solution, pentlandite $(Fe,Ni)_9S_8$, and/or Fe-Ni alloy.[2] On the basis of the high temperature phase relations, pentlandite and the associated alloy phase do not appear to be high temperature phases and thus must form during cooling.

In order to explore the effect of cooling, a vertical section through the ternary Fe-Ni-S composition-temperature phase relationships was developed and is shown in Fig. 14. A fundamental difference between the vertical sections in a ternary system and the equivalent binary system is that, in

general, the liquidus and solidus lines in vertical sections are not conjugate lines as they are in the binary phase diagram. Also the horizontal lines joining the composition of conjugate liquid and solid phases are not tie lines. At a temperature of 1150 K and sulfur pressure of 1.4×10^{-2} Nm^{-2} the composition of OL-II containing Fe, Ni and S will lie on section a-b shown in Fig. 14. At this temperature the OL-II is composed of $(Ni,Fe)S_{1-x}(l)$ with small amounts of iron-rich $(Fe,Ni)_{1-x}S$ solid solution. On cooling $(Ni,Fe)_{3\pm x}S_2$ begins to crystallize from the liquid sulfide melt, until all the liquid phase is used up. The changes in composition caused by a further decrease in temperature results in the precipitation of some Fe-Ni alloy. Below 850 K pentlandite begins to form as a solid phase from $(Fe,Ni)_{1-x}S$ and $(Ni,Fe)_{3\pm x}S_2$. The formation of pentlandite appears to be extremely rapid and cannot be prevented by quenching the corroded samples. This sample clearly demonstrates the necessity for high temperature stability field diagrams for the interpretation of corrosion behavior on the basis of corrosion products observed after cooling the corroded specimen to room temperature.

SUMMARY

The sulfur potential diagrams were developed for the ternary systems of Fe-Cr-S, Fe-Ni-S and Ni-Cr-S and the quarternary system of Fe-Cr-Ni-S. At high temperatures these systems contain ternary compounds and solid solutions for which thermodynamic data are not available. The free energies of formation were estimated using current models and correlations along with available information on phase relations in other ternary systems that exist mainly in the geophysical literature. Conflicts in existing data on some

binary compounds are discussed and values consistent with ternary phase relations and empirical correlations were selected. Based on these thermodynamic evaluations, sulfur potential diagrams were constructed. The calculated stability phase fields were compared with sulfide phases and compositions obtained experimentally following the dynamic sulfidating of SAE 310 stainless steel. Since the composition of the sulfide scales often controls the kinetics of sulfidation, the ability to predict the structure and composition of these phases are a significant step forward in the understanding of corrosion behavior and in the design of alloys for specific sulfur environments.

ACKNOWLEDGMENTS

The authors wish to thank Dr. Ian Finnie and Mr. A. V. Levy for their support and encouragement. Financial support from the Materials and Physical Sciences Branch of Ames Research Center, NASA, through the grant NCA2-OR050-706, and from Physical Research Division of ERDA is gratefully acknowledged.

REFERENCES

1. D. Bhogeswara Rao and Howard G. Nelson, Sulfidation of SAE 310 Stainless Steel at Sulfur Potentials Encountered in Coal Conversion Systems, NASA Technical Memorandum, NASA TM X-73,166, September 1976, and the Proceedings of the Symposium on Properties of High Temperature Alloys, eds. Z. A. Foroulis and F. S. Pettit, Proceedings Vol. 77-1, The Electrochemical Soc., Inc., Princeton, NJ, 464 (1971).

2. D. Bhogeswara Rao and H. G. Nelson, Oxidation of Metals, in press.

3. D. Lundquist, *Ark. Kemi. Mineral. Geol.*, 24A, No. 22 (1947).

4. G. Kullerud, Carnegie Inst. Wash. Yearbook, 175 (1963).

5. A. J. Naldrett, J. R. Craig, and G. Kullerud, *Econ. Geol.*, 62, 826 (1967).

6. J. R. Craig, A. J. Naldrett, and G. Kullerud, Carnegie Inst. Wash. Yearbook, 440 (1968).

7. G. Kullerud, R. A. Yund, and G. H. Moh, *Econ. Geol. Monogr.*, 4, 323 (1969).

8. R. W. Shewman and Y. A. Clark, *Can. J. Earth Sci.*, 7, 67 (1970).

9. J. R. Craig, Carnegie Inst. Wash. Yearbook, 66, 434 (1968).

10. J. R. Craig, *Am. Mineral*, 56, 1303 (1971).

11. J. R. Craig, *Am. J. Sci.*, 273A, 496 (1973).

12. K. C. Misra and M. E. Fleet, *Mat. Res. Bull.*, 8, 669 (1973).

13. K. C. Misra and M. E. Fleet, *Econ. Geol.*, 69, 391 (1974).

14. A. El Goresy and G. Kullerud, Carnegie Inst. Wash. Yearbook, 182 (1969).

15. A. El Goresy and G. Kullerud, *Meteorite Research*, ed., P. M. Millman, Reidel Publishing Company, Dordrecht, Holland, 638 (1969).

16. M. Hansen and K. Anderko, *Constitution of Binary Alloys*, McGraw-Hill Book Co., New York, 1958, p. 704.

17. T. Uno, K. Kanbara, E. Homma, *Tetsu-to-Hagane*, 36, 479 (1950).

18. E. T. Turkdogan, *Trans. A.I.M.E.*, 242, 1665 (1968).

19. T. Rosenquist, *J. Iron Steel Inst.*, 176, 37 (1954).

20. G. Urbain, W. Burgmann, and M. G. Frohberg, *C. R. hebd. Seane. Acad. Sci.*, Paris, Ser C. 263, 595 (1966).

21. K. C. Mills, *Thermodynamic Data for Inorganic Sulfides, Selenides and Tellurides*, Butterworths, London (1974).

22. F. Jellinek, *Acta Crystallogr.*, 10, 620 (1957).

23. T. J. A. Popma and C. F. van Bruggen, *J. Inorg. Nucl. Chem.*, 31, 73 (1969).

24. J. P. Hager and J. F. Elliott, *Trans. Met. Soc. A.I.M.E*, 239, 513 (1967).

25. D. J. Young, W. W. Smeltzer, and J. S. Kirkaldy, *J. Electrochem. Soc.*, 120, 1221 (1973).

26. O. Kubaschewski, E. L. Evans, and C. B. Alcock, *Metallurgical Thermochemistry*, Pergamon Press, New York (1967).

27. K. Igaki, N. Ohashi, and M. Mikami, *J. Phys. Soc. Japan*, 31, 1424 (1971).

28. K. Nishida, K. Nakayama, and T. Narita, *Corros. Sci.*, 13, 759 (1973).

29. J. R. Craig and S. D. Scott, Sulfide Mineralogy, ed. P. H. Ribbe, Short Course Notes, Vol. 1, p. CS1, Mineralogical Society of America, Washington, D. C. (1974).

30. M. Nagamori and T. R. Ingraham, *Met. Trans.*, 1, 1821 (1970).

31. G. A. Meyer, J. S. Warner, Y. K. Rao, and H. H. Kellogg, *Met. Trans.* B, 6B, 229 (1975).

32. H. Rau, *J. Phys. Chem. Solids*, 36, 1199 (1975).

33. H. Rau, *J. Phys. Chem. Solids*, 37, 929 (1976).

34. G. Line and M. Laffitte, *C. R. Acad. Sci. Paris*, 256, 3306 (1963).

35. R. Y. Lin, D. Hu, and Y. A. Chang, *Met. Trans. B* (in press).

36. B. R. Conrad, R. Sridhar, and J. S. Warner, High Temperature Enthalpies of Nickel Sulfides, Presented at 106th Annual AIME Meeting, Atlanta, Georgia (1977).

37. H. K. Hardy, *Acta Met.*, 1, 203 (1953).

38. R. Hultgren, P. D. Desai, D. T. Hawkins, M. Gleiser, and K. K. Kelley, Selected Values of the Thermodynamic Properties of Binary Alloys, ASM, Metals Park, Ohio (1973).

39. J. A. Kessler, Yu D. Tretyakov, I. V. Gordeyer and V. A. Alferov, *J. Chem. Thermodyn.*, 8, 10 (1976).

40. R. Vogel and Th. Heumann, *Neues Jahrb. Mineral. Monatsh.*, 175 (1950).

41. J. F. Counsell, E. B. Lees, and P. J. Spencer, in Metallurgical Chemistry Symposium, ed. O. Kubaschewski, HMSO, London, 451 (1972).

42. H. Gaye and C. H. P. Lupis, *Scripta Mets.*, 4, 685 (1970).

43. B. Carnhan, H. A. Luther, and J. O. Wilkes, *Applied Numerical Methods*, John Wiley, New York (1969).

44. P. M. Bell, J. L. England, and G. Kullerud, Carnegie Inst. Wash. Yearbook, 63, 206 (1964).

45. J. S. Kirdaldy, G. M. Bolze, D. McCutcheon, and D. J. Young, *Met. Trans.*, 4, 1519 (1973).

46. K. T. Jacob, *J. Solid State Chemistry*, Nov. 1977, in press.

47. A. Navrotsky and O. J. Kleppa, *J. Inorg. Nucl. Chem.*, 30, 479 (1968).

48. K. T. Jacob and C. B. Alcock, *Met. Trans. B*, 6B, 215 (1975).

49. K. T. Jacob and C. B. Alcock, *J. Am. Ceram. Soc.*, 8, 192 (1975).

50. K. T. Jacob, *Thermochimica Acta*, 15, 79 (1976).

51. K. T. Jacob, unpublished research.

52. K. T. Jacob and K. Fitzner, *Thermochimica Acta*, 18, 197 (1977).

53. K. T. Jacob and C. B. Alcock, *J. Solid State Chem.*, 20, 79 (1977).

TABLE 1. COMPARISON OF REPORTED VALUES FOR THE STANDARD GIBB'S FREE ENERGY OF FORMATION OF METAL SATURATED $Cr_{1-x}S$ PHASE AT 973 K

Investigator	$\Delta G°$, kJ $mole^{-1}$	Experimental technique
Hager and Elliott[24]	-148 (±2)	Gas equilibrium
Young, Smeltzer, and Kirkaldy[25]	-140 (±8.5)	Gas equilibrium
El Goresy and Kullerud[15]		
Simple analysis assuming that the monosulfide phase behaves as pseudo-binary system	-112 (±3.5)	Phase diagram determination by X-ray analysis
Complex analysis that corrects for the varying sulfur concentration of the monosulfide solid solution	-120 (±4)	
Selected value	-133 (±10)	

NOMENCLATURE

a_i	activity of component i
ΔG^o	standard Gibb's free energy change
ΔG^M	integral molar free energy of mixing
ΔG_i^o	partial molar free energy of mixing of component i
ΔH	standard enthalpy change
ΔH_i	partial molar enthalpy (heat) of mixing of component i
ΔH^M	integral molar enthalpy (heat) of mixing
K	equilibrium constant
n_i	moles of component i
P_{S_2}	partial pressure of diatomic sulfur
R	gas constant
ΔS_i	partial molar entropy of mixing of component i
ΔS^M	integral molar entropy of mixing
ΔS^o	standard entropy change
T or K	absolute temperature
X_i	mole fraction of component i
γ_i	activity coefficient of component i
$\Delta\mu_i$	relative chemical potential of component i

FIGURE CAPTIONS

Fig. 1. Stability fields in the Fe-Cr-S system at 1275 K as a function of log P_{S_2}.

Fig. 2. Gibb's triangle representation of phase relations in the Fe-Cr-S system at 973 K.[14,15]

Fig. 3. The stability fields in the Fe-Cr-S system at 1065 K as a function of P_{S_2}.

Fig. 4. The stability fields in the Fe-Cr-S system at 900 K as a function of P_{S_2}.

Fig. 5. Effect of temperature on the stability fields of various phases in the Fe-Cr-S system at a fixed sulfur partial pressure ($P_{S_2} = 10^{-2}$ Nm^{-2}).

Fig. 6. Stability fields in the Fe-Ni-S system at 1275 K as a function of P_{S_2}.

Fig. 7. Stability fields in the Fe-Ni-S system at 1150 K as a function of P_{S_2}.

Fig. 8. Stability fields in the Fe-Ni-S system at 900 K as a function of P_{S_2}.

Fig. 9. The effect of temperature on the stability fields in the Fe-Ni-S system at a constant partial pressure of sulfur ($P_{S_2} = 10^{-2}$ Nm^{-2}).

Fig. 10. Stability fields in the Ni-Cr-S system at 1275 K as a function of P_{S_2}.

Fig. 11. The sulfide phases and their compositions at 1275 K that form on SAE 310 stainless steel under equilibrium (powdered alloy) and nonequilibrium (bulk sample) conditions at different sulfur partial pressures.

Fig. 12. Compositional analysis of specimen corroded at 933 K showing spinel phase OL-II/OL-I/subscale/alloy.

Fig. 13. Microstructure of a monosulfide $(Fe,Ni)_{1-x}S$ solid phase growing out of an initially thin film of liquid melt ($(Fe,Ni)S_{1-x}(\ell)$).

Fig. 14. A vertical section through the Fe-Ni-S composition-temperature phase diagram. The composition of OL-II at 1150 K and $P_{S_2} = 1.4 \times 10^{-2}$ Nm^{-2} falls on the section a-b. The points a and b are the compositions of the binary Fe-S and Ni-S phases that exist at 1150 K and $P_{S_2} = 1.4 \times 10^{-2}$ Nm^{-2}.

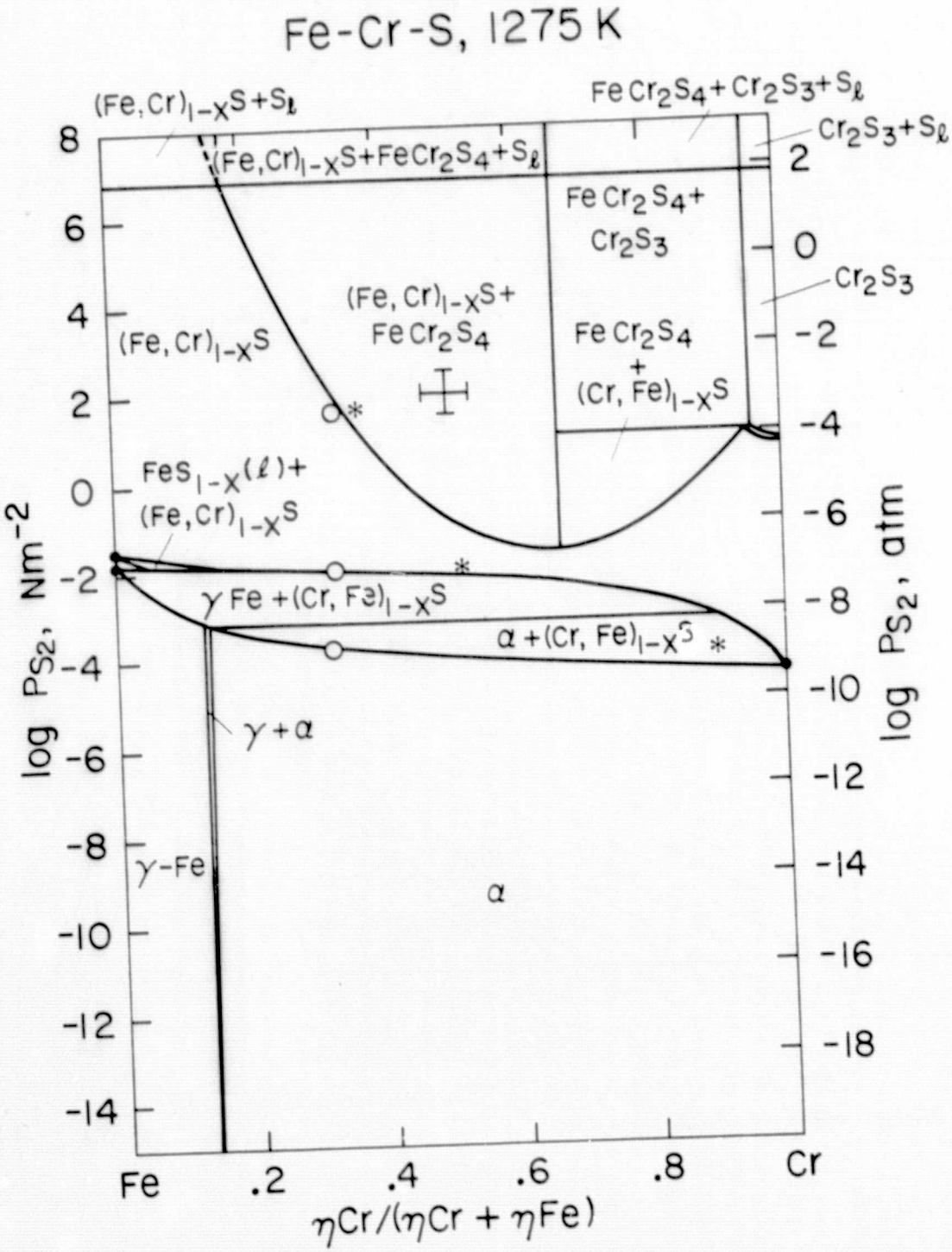
Fe-Cr-S, 1275 K
(Fe,Cr)1-xS+Sℓ
FeCr2S4+Cr2S3+Sℓ
Cr2S3+Sℓ
(Fe,Cr)1-xS+FeCr2S4+Sℓ
FeCr2S4+
Cr2S3
Cr2S3
(Fe,Cr)1-xS+
FeCr2S4
(Fe,Cr)1-xS
FeCr2S4
+
(Cr,Fe)1-xS
FeS1-x(ℓ)+
(Fe,Cr)1-xS
γ Fe +(Cr,Fe)1-xS
α +(Cr,Fe)1-xS
γ+α
γ-Fe
α
log PS2, Nm-2
log PS2, atm
Fe
Cr
ηCr/(ηCr + ηFe)

Fig. 1

ORIGINAL PAGE IS
OF POOR QUALITY

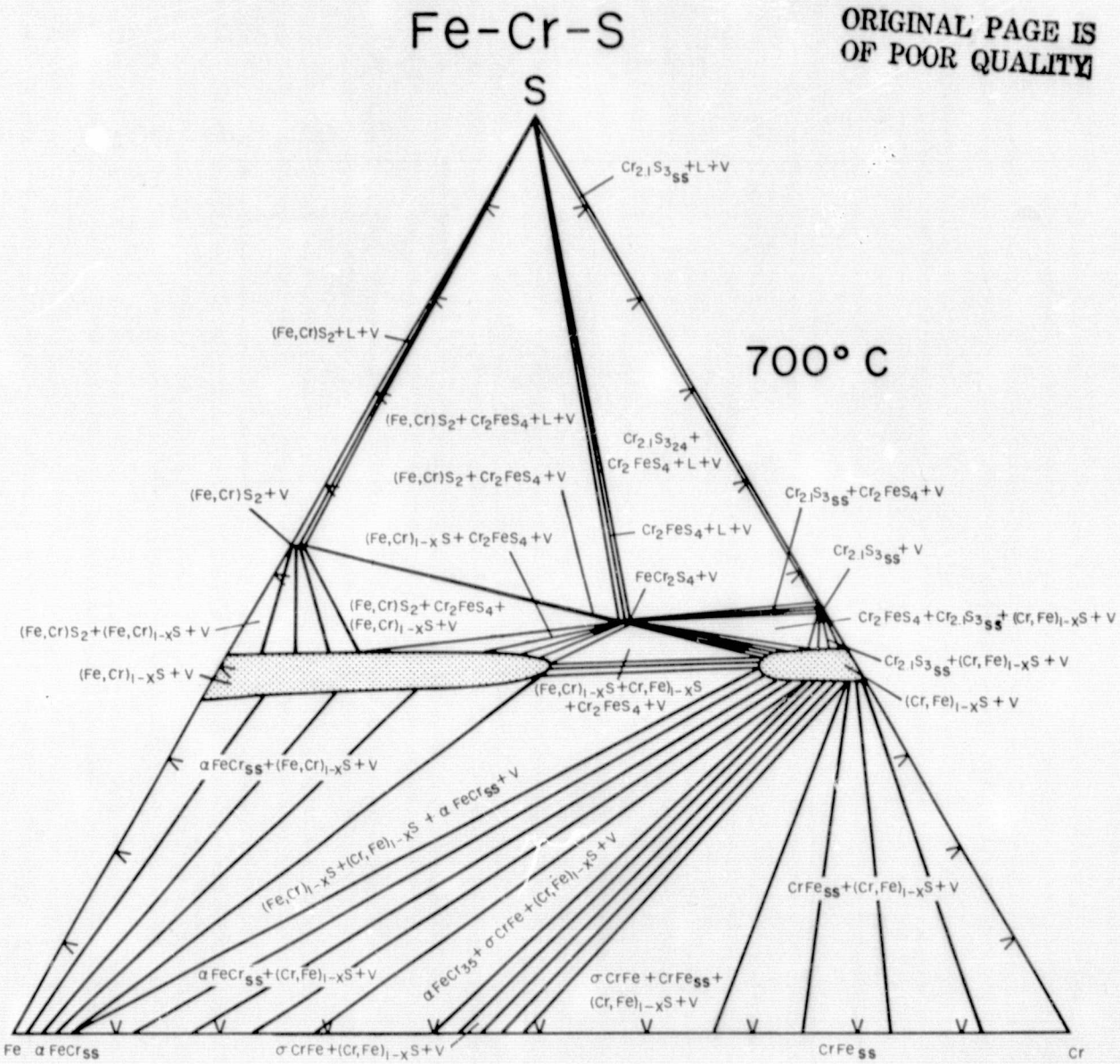

A. EL GORESY AND G. KULLERUD, CARNEGIE INSTITUTE OF WASHINGTON YEAR BOOK, p. 185, 1964

Fig. 2

ORIGINAL PAGE IS
POOR QUALITY

ORIGINAL PAGE IS
OF POOR QUALITY

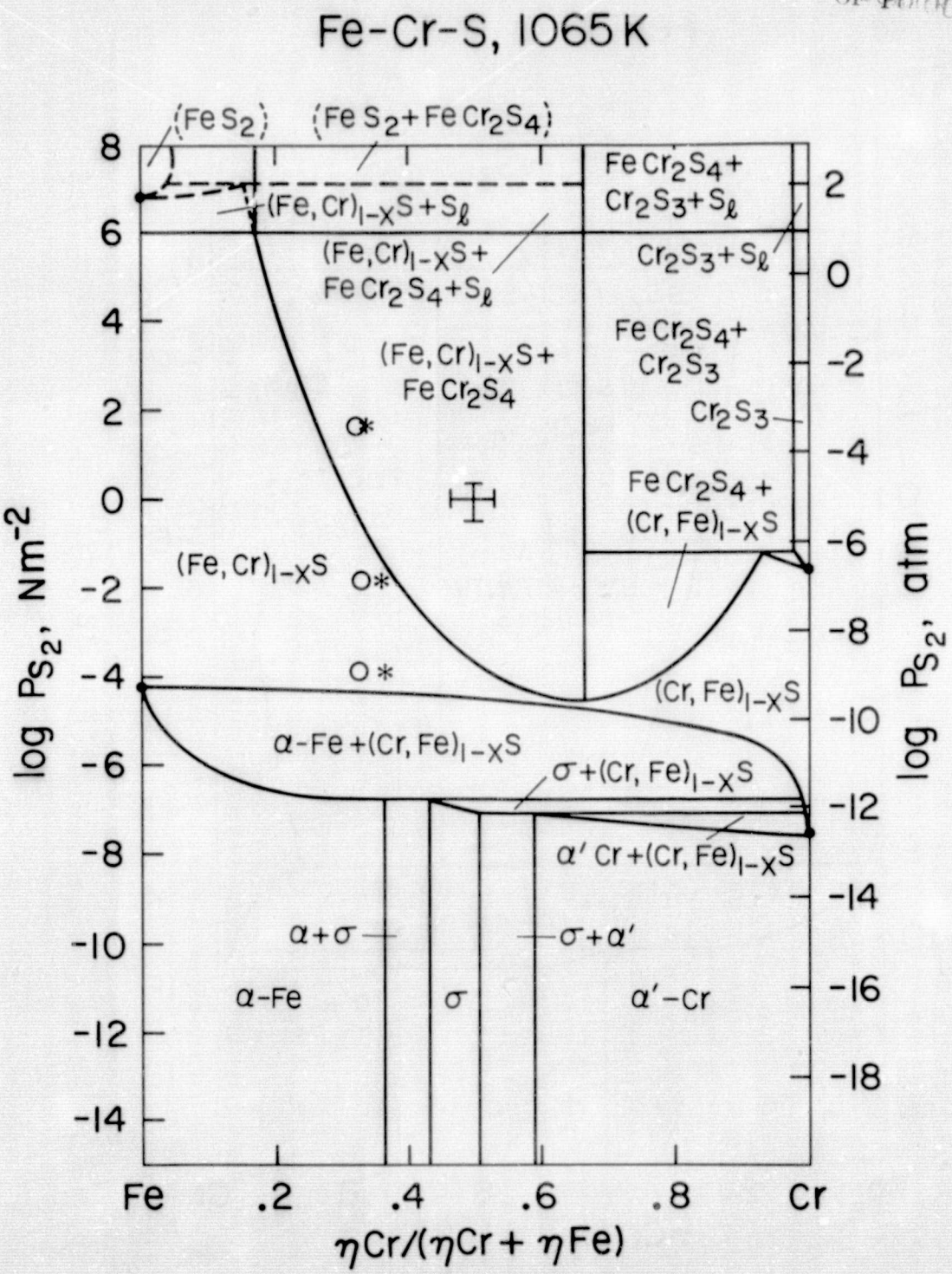

Fig. 3

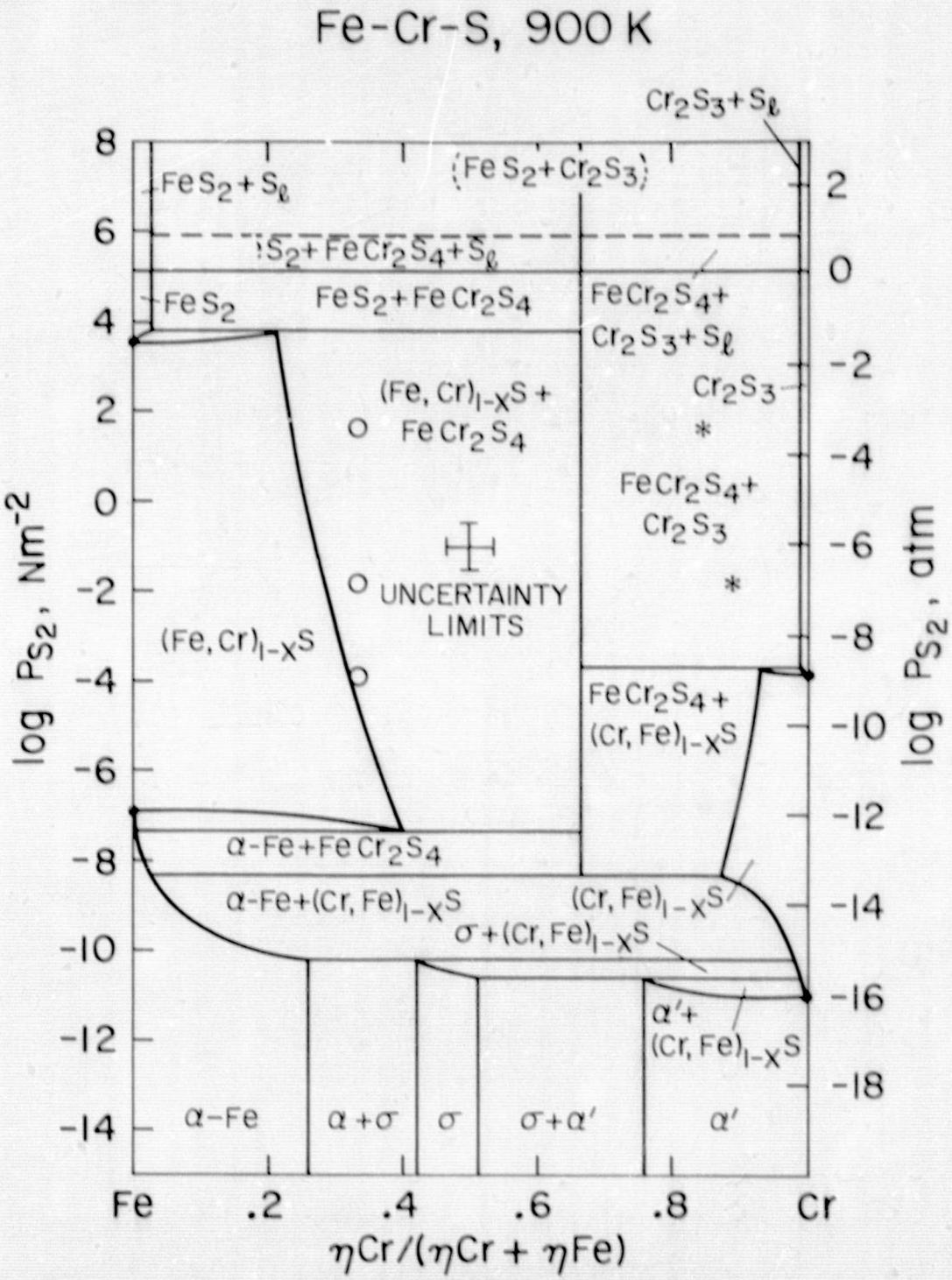
Fe-Cr-S, 900 K
$Cr_2S_3+S_\ell$
FeS_2+S_ℓ
$(FeS_2+Cr_2S_3)$
$S_2+FeCr_2S_4+S_\ell$
FeS_2
$FeS_2+FeCr_2S_4$
$FeCr_2S_4+$
$Cr_2S_3+S_\ell$
$(Fe,Cr)_{1-x}S+$
$FeCr_2S_4$
Cr_2S_3
$FeCr_2S_4+$
Cr_2S_3
UNCERTAINTY
LIMITS
$(Fe,Cr)_{1-x}S$
$FeCr_2S_4+$
$(Cr,Fe)_{1-x}S$
α-Fe+$FeCr_2S_4$
α-Fe+$(Cr,Fe)_{1-x}S$
$(Cr,Fe)_{1-x}S$
$\sigma+(Cr,Fe)_{1-x}S$
$\alpha'+$
$(Cr,Fe)_{1-x}S$
α-Fe
$\alpha+\sigma$
σ
$\sigma+\alpha'$
α'
log P_{S_2}, Nm^{-2}
log P_{S_2}, atm
Fe
Cr
$\eta Cr/(\eta Cr+\eta Fe)$

Fig. 4

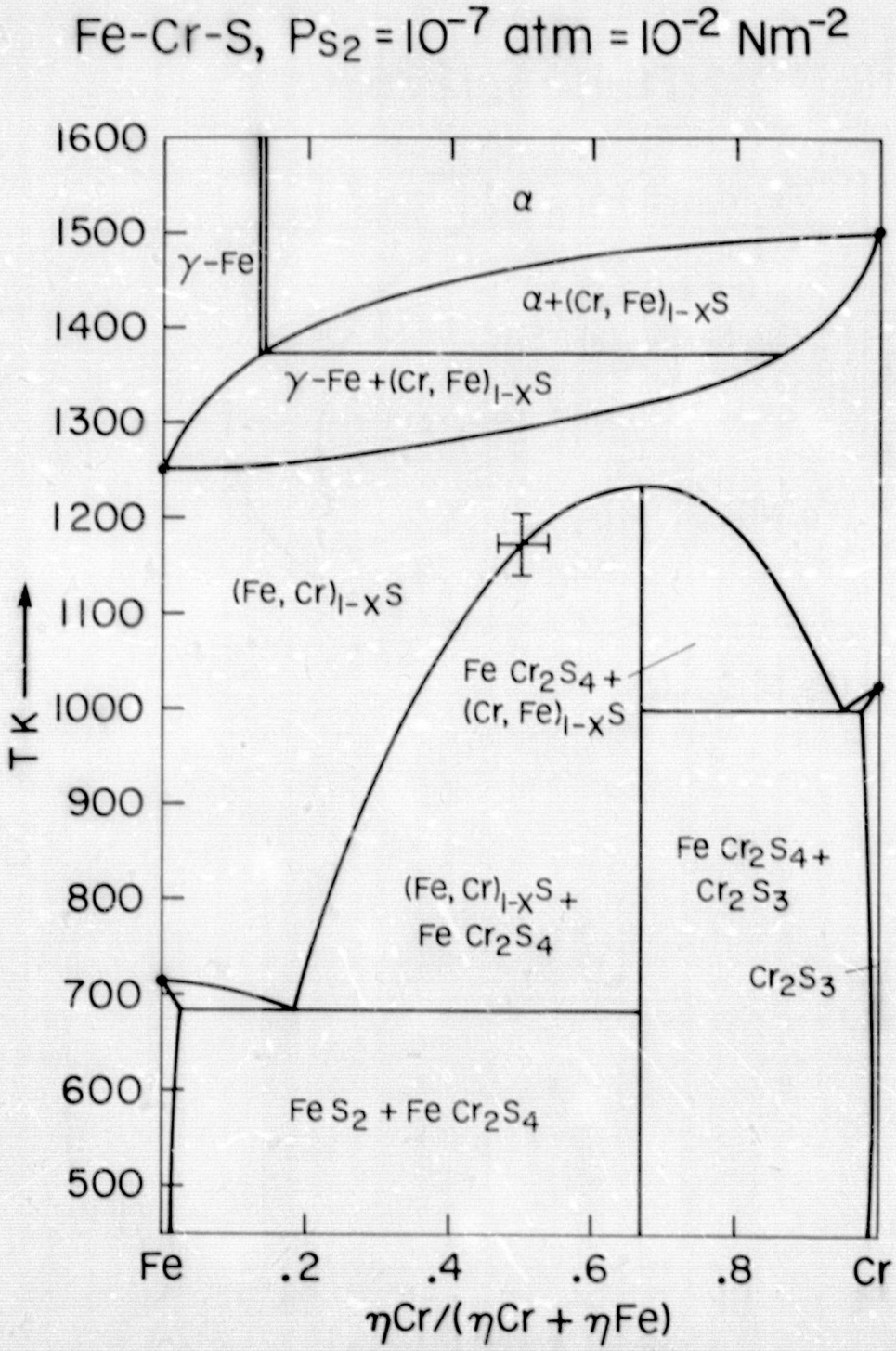
Fe-Cr-S, $P_{S_2} = 10^{-7}$ atm = 10^{-2} Nm^{-2}
1600
1500
1400
1300
1200
1100
1000
900
800
700
600
500
T K
α
γ-Fe
α+(Cr, Fe)$_{1-x}$S
γ-Fe +(Cr, Fe)$_{1-x}$S
(Fe, Cr)$_{1-x}$S
Fe Cr_2S_4 +
(Cr, Fe)$_{1-x}$S
(Fe, Cr)$_{1-x}$S +
Fe Cr_2S_4
Fe Cr_2S_4+
Cr_2S_3
Cr_2S_3
Fe S_2 + Fe Cr_2S_4
Fe
.2
.4
.6
.8
Cr
ηCr/(ηCr + ηFe)

Fig. 5

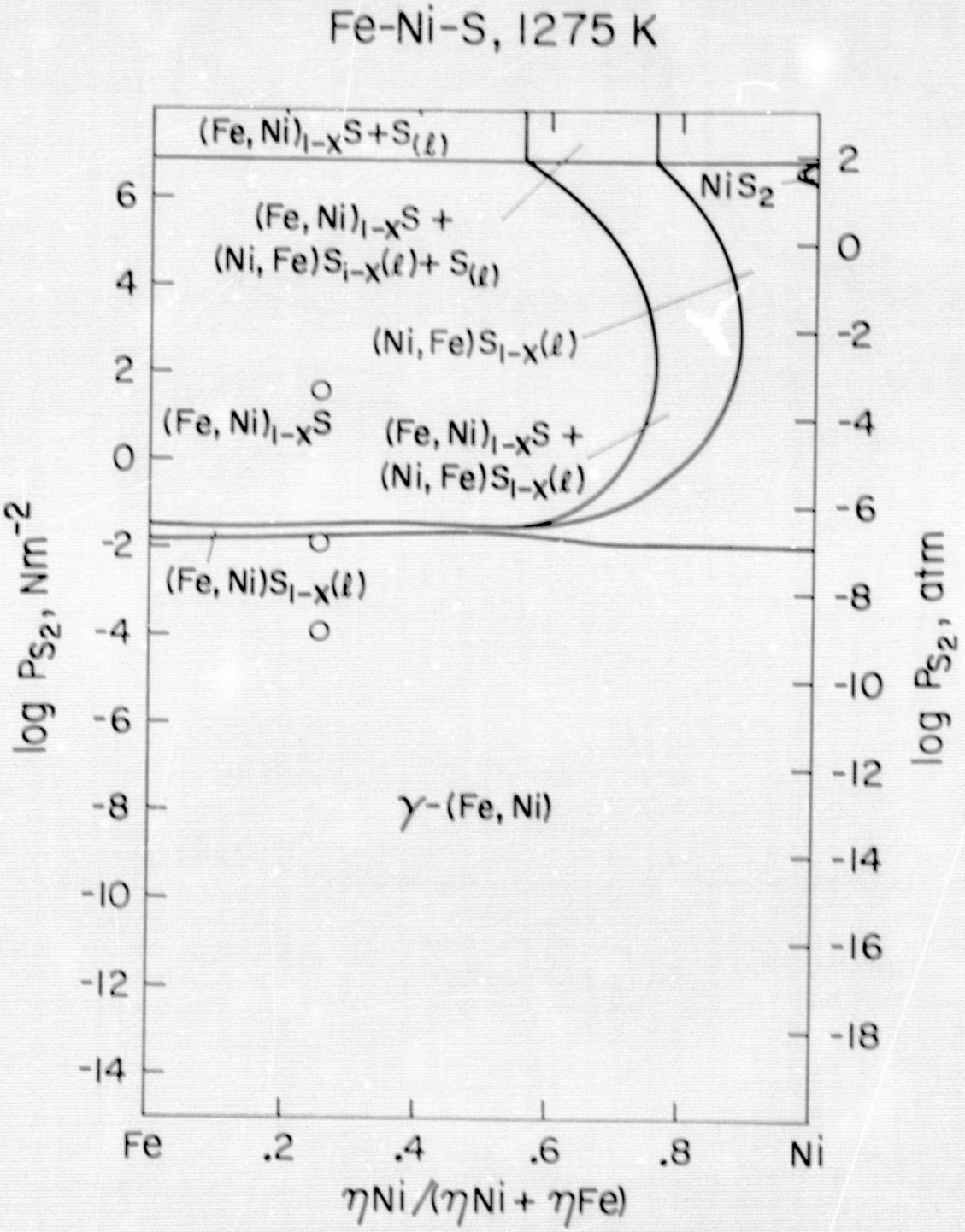
Fe-Ni-S, 1275 K
(Fe, Ni)$_{1-x}$S+S$_{(\ell)}$
NiS$_2$
(Fe, Ni)$_{1-x}$S +
(Ni, Fe)S$_{1-x}$(ℓ)+ S$_{(\ell)}$
(Ni, Fe)S$_{1-x}$(ℓ)
(Fe, Ni)$_{1-x}$S
(Fe, Ni)$_{1-x}$S +
(Ni, Fe)S$_{1-x}$(ℓ)
(Fe, Ni)S$_{1-x}$(ℓ)
γ-(Fe, Ni)
log P$_{S_2}$, Nm^{-2}
log P$_{S_2}$, atm
6
4
2
0
-2
-4
-6
-8
-10
-12
-14
2
0
-2
-4
-6
-8
-10
-12
-14
-16
-18
Fe
.2
.4
.6
.8
Ni
ηNi/(ηNi + ηFe)

Fig. 6

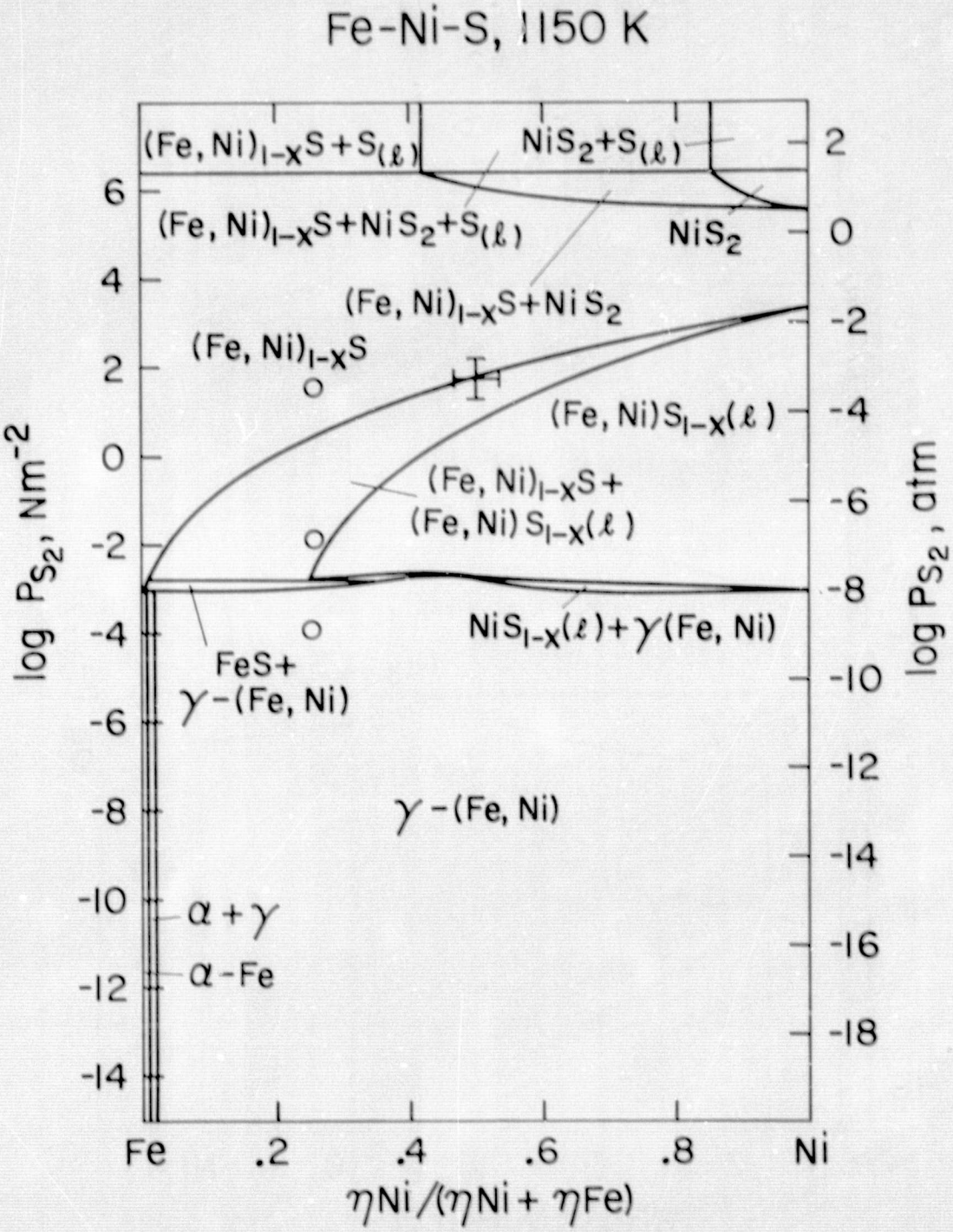
Fe-Ni-S, 1150 K
(Fe, Ni)$_{1-x}$S + S$_{(\ell)}$
NiS$_2$+S$_{(\ell)}$
(Fe, Ni)$_{1-x}$S+NiS$_2$+S$_{(\ell)}$
NiS$_2$
(Fe, Ni)$_{1-x}$S+NiS$_2$
(Fe, Ni)$_{1-x}$S
(Fe, Ni)S$_{1-x}$(ℓ)
(Fe, Ni)$_{1-x}$S+
(Fe, Ni)S$_{1-x}$(ℓ)
NiS$_{1-x}$(ℓ)+γ(Fe, Ni)
FeS+
γ-(Fe, Ni)
γ-(Fe, Ni)
$\alpha+\gamma$
α-Fe
log P$_{S_2}$, Nm^{-2}
log P$_{S_2}$, atm
Fe
.2
.4
.6
.8
Ni
ηNi/(ηNi + ηFe)

Fig. 7

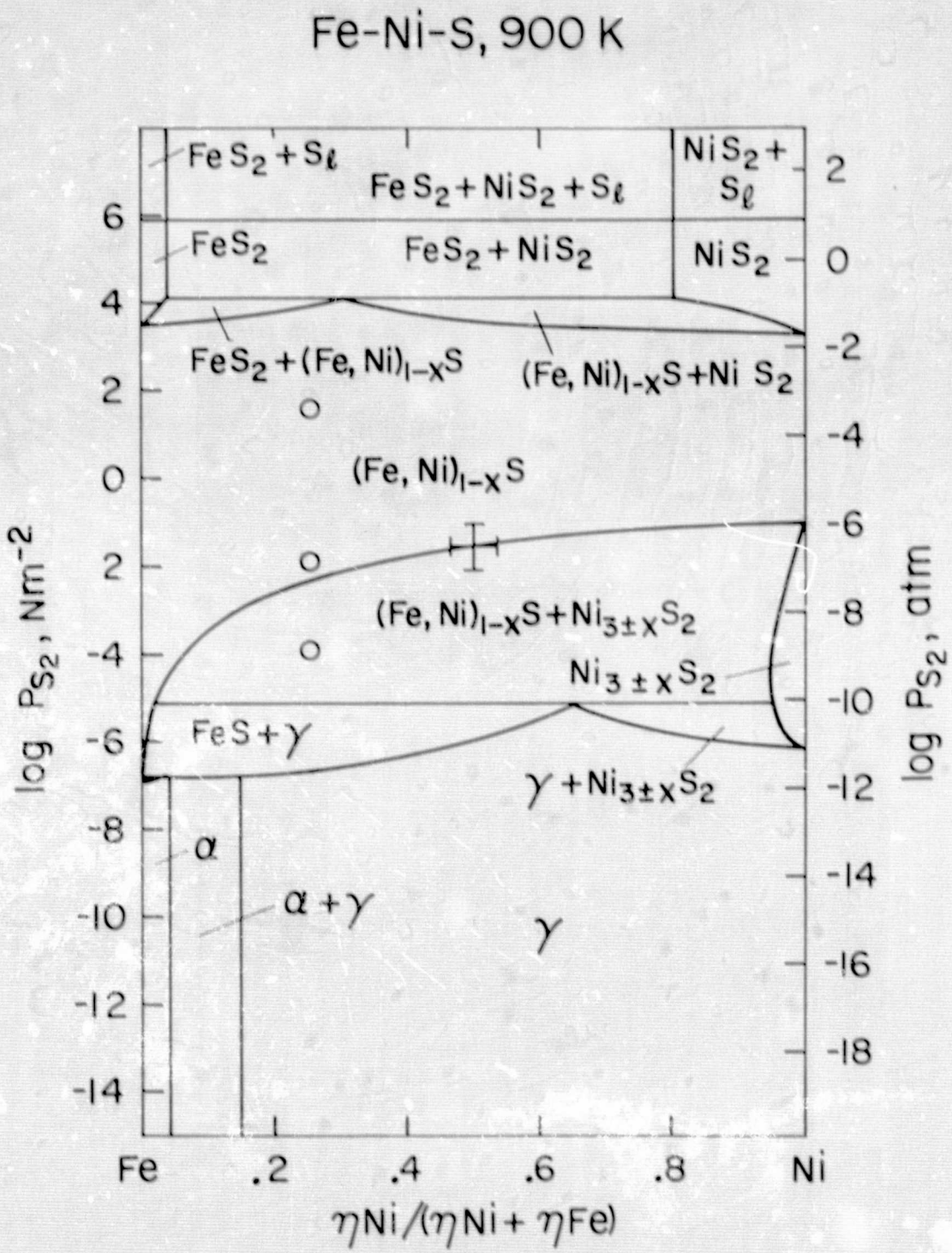
Fe-Ni-S, 900 K
FeS2 + Sℓ
FeS2 + NiS2 + Sℓ
NiS2 + Sℓ
FeS2
FeS2 + NiS2
NiS2
FeS2 + (Fe, Ni)1-xS
(Fe, Ni)1-xS + NiS2
(Fe, Ni)1-xS
(Fe, Ni)1-xS + Ni3±xS2
Ni3±xS2
FeS + γ
γ + Ni3±xS2
α
α + γ
γ
log PS2, Nm-2
log PS2, atm
Fe
.2
.4
.6
.8
Ni
ηNi/(ηNi + ηFe)

Fig. 8

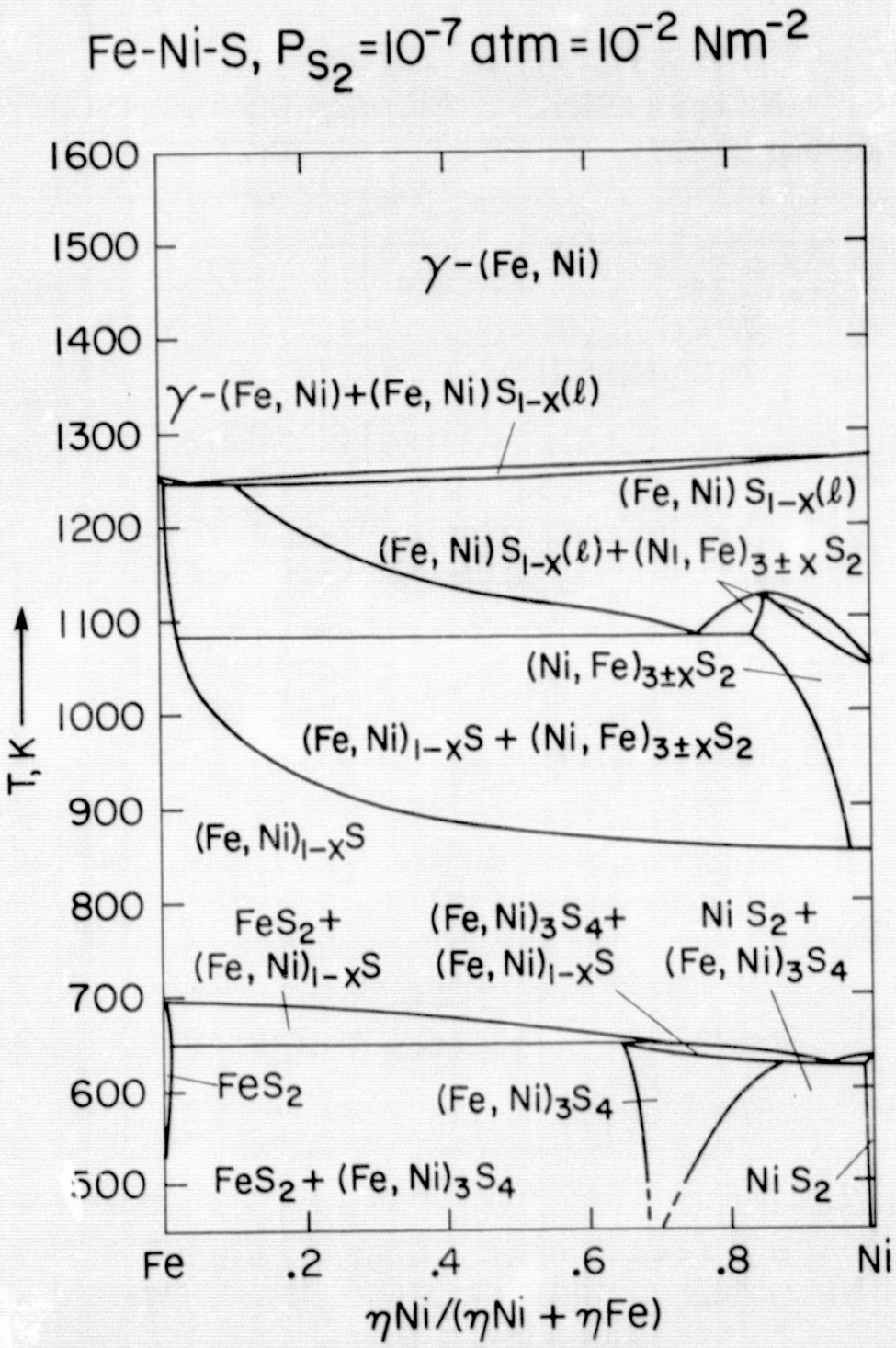
Fe-Ni-S, $P_{S_2} = 10^{-7}$ atm $= 10^{-2}$ Nm^{-2}
1600
1500
1400
1300
1200
1100
1000
900
800
700
600
500
T, K
γ-(Fe, Ni)
γ-(Fe, Ni)+(Fe, Ni) $S_{1-x}(\ell)$
(Fe, Ni) $S_{1-x}(\ell)$
(Fe, Ni) $S_{1-x}(\ell)$+(Ni, Fe)$_{3\pm x}S_2$
(Ni, Fe)$_{3\pm x}S_2$
(Fe, Ni)$_{1-x}$S + (Ni, Fe)$_{3\pm x}S_2$
(Fe, Ni)$_{1-x}$S
FeS_2+ (Fe, Ni)$_{1-x}$S
(Fe, Ni)$_3S_4$+ (Fe, Ni)$_{1-x}$S
Ni S_2 + (Fe, Ni)$_3S_4$
FeS_2
(Fe, Ni)$_3S_4$
FeS_2+ (Fe, Ni)$_3S_4$
Ni S_2
Fe
.2
.4
.6
.8
Ni
ηNi/(ηNi + ηFe)

Fig. 9

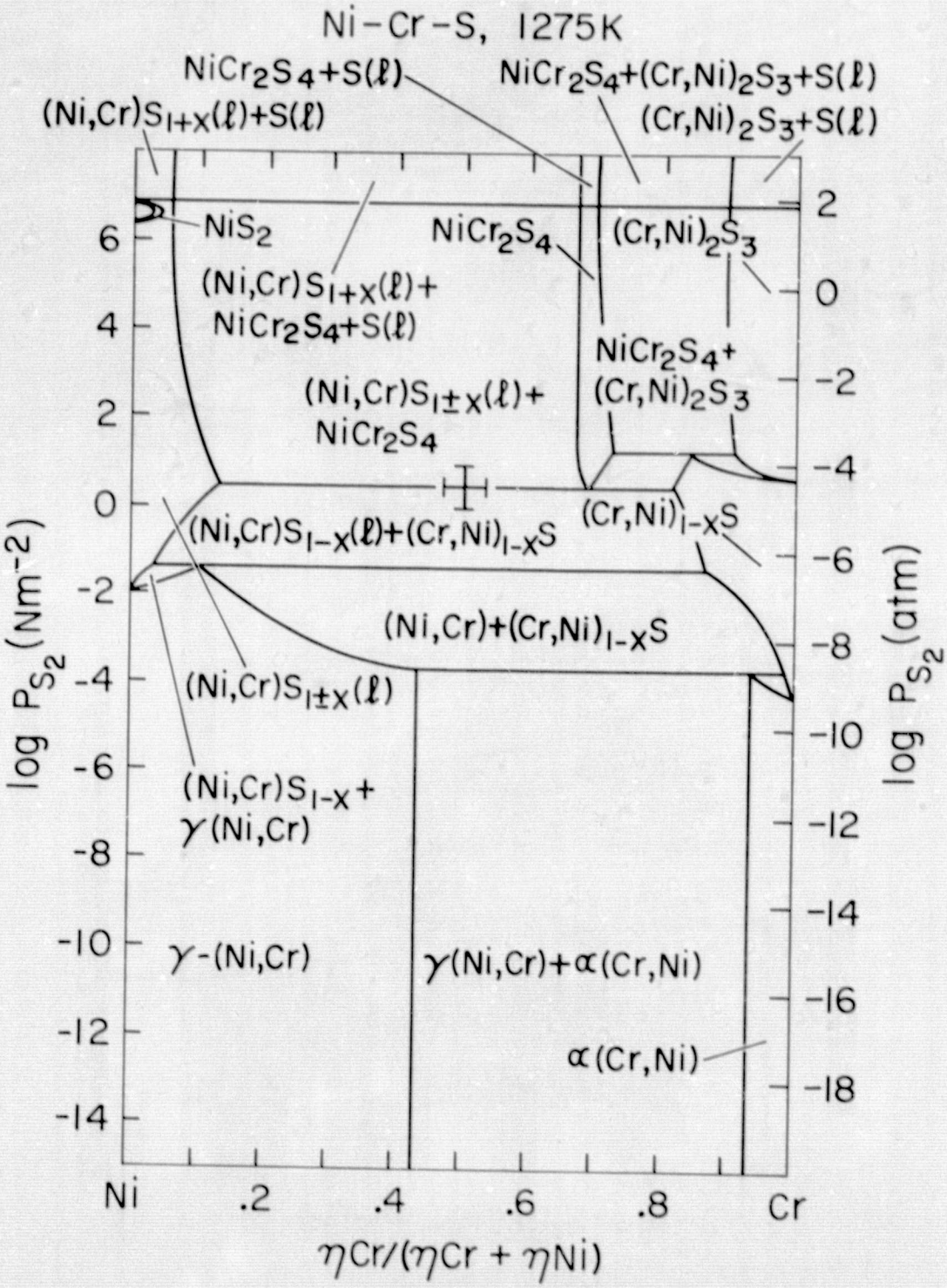
Ni-Cr-S, 1275K
NiCr2S4+S(ℓ)
NiCr2S4+(Cr,Ni)2S3+S(ℓ)
(Ni,Cr)S1+x(ℓ)+S(ℓ)
(Cr,Ni)2S3+S(ℓ)
NiS2
NiCr2S4
(Cr,Ni)2S3
(Ni,Cr)S1+x(ℓ)+
NiCr2S4+S(ℓ)
NiCr2S4+
(Cr,Ni)2S3
(Ni,Cr)S1±x(ℓ)+
NiCr2S4
(Cr,Ni)1-xS
(Ni,Cr)S1-x(ℓ)+(Cr,Ni)1-xS
(Ni,Cr)+(Cr,Ni)1-xS
(Ni,Cr)S1±x(ℓ)
(Ni,Cr)S1-x+
γ(Ni,Cr)
γ-(Ni,Cr)
γ(Ni,Cr)+α(Cr,Ni)
α(Cr,Ni)
log PS2 (Nm-2)
log PS2 (atm)
Ni
.2
.4
.6
.8
Cr
ηCr/(ηCr + ηNi)

Fig. 10

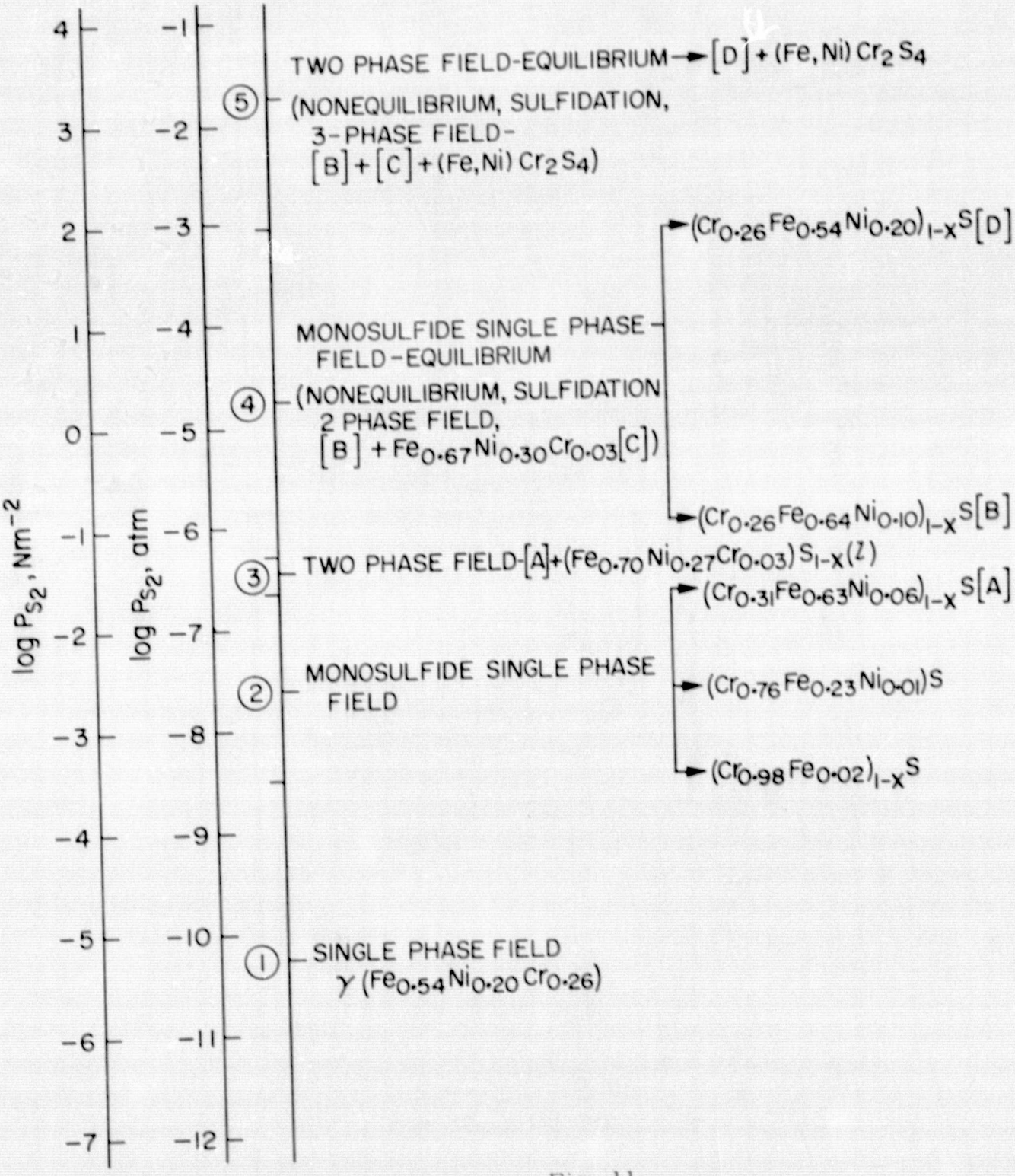
log P_{S_2}, Nm^{-2}
log P_{S_2}, atm
4
3
2
1
0
-1
-2
-3
-4
-5
-6
-7
-1
-2
-3
-4
-5
-6
-7
-8
-9
-10
-11
-12
5
TWO PHASE FIELD-EQUILIBRIUM → [D] + (Fe, Ni) Cr_2S_4
(NONEQUILIBRIUM, SULFIDATION,
3-PHASE FIELD-
[B] + [C] + (Fe,Ni) Cr_2S_4)
$(Cr_{0.26}Fe_{0.54}Ni_{0.20})_{1-x}S$[D]
MONOSULFIDE SINGLE PHASE
FIELD-EQUILIBRIUM
4
(NONEQUILIBRIUM, SULFIDATION
2 PHASE FIELD,
[B] + $Fe_{0.67}Ni_{0.30}Cr_{0.03}$[C])
$(Cr_{0.26}Fe_{0.64}Ni_{0.10})_{1-x}S$[B]
3
TWO PHASE FIELD-[A]+$(Fe_{0.70}Ni_{0.27}Cr_{0.03})S_{1-x}(l)$
$(Cr_{0.31}Fe_{0.63}Ni_{0.06})_{1-x}S$[A]
2
MONOSULFIDE SINGLE PHASE
FIELD
$(Cr_{0.76}Fe_{0.23}Ni_{0.01})S$
$(Cr_{0.98}Fe_{0.02})_{1-x}S$
1
SINGLE PHASE FIELD
γ $(Fe_{0.54}Ni_{0.20}Cr_{0.26})$

Fig. 11

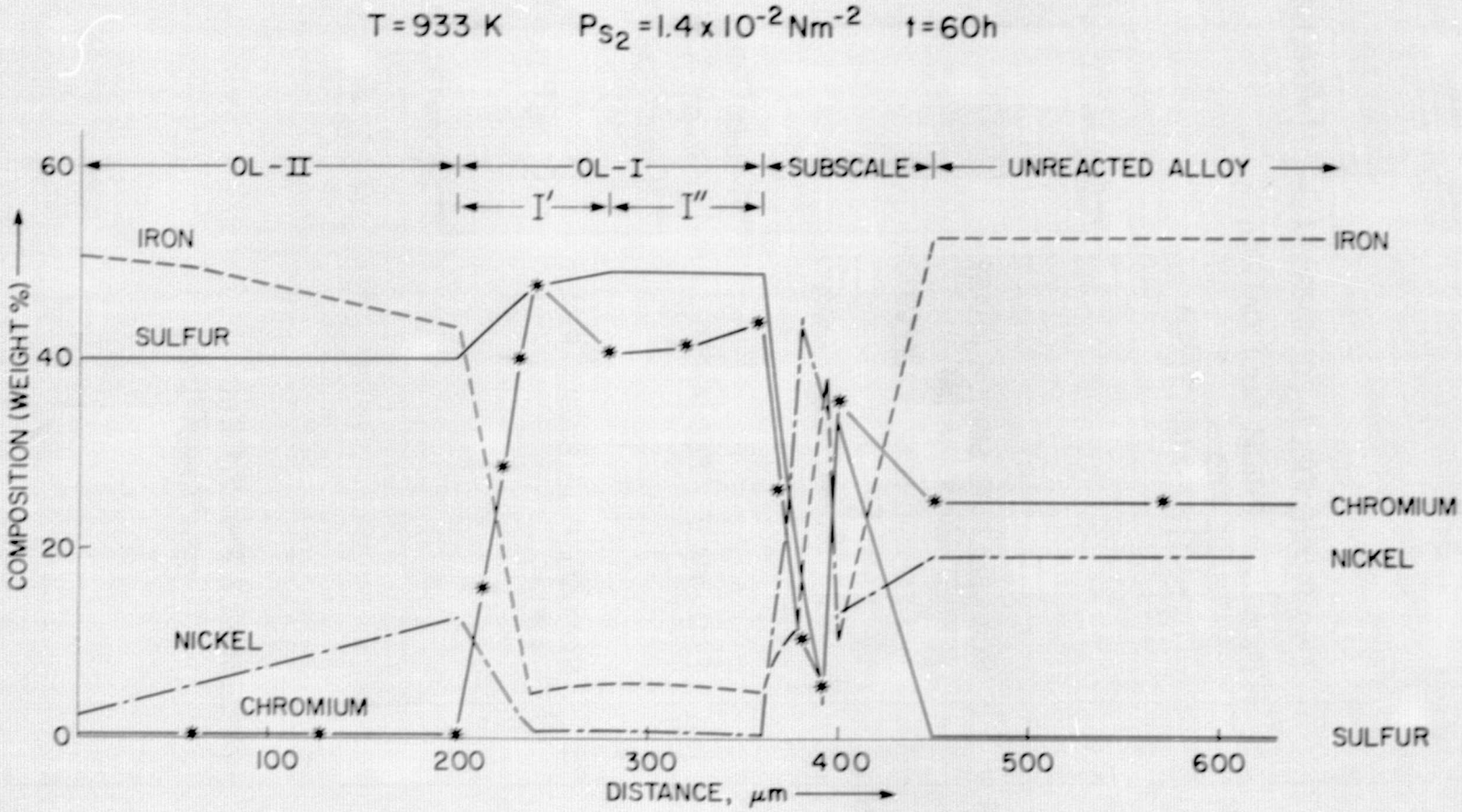
T = 933 K
$P_{S_2} = 1.4 \times 10^{-2}\ Nm^{-2}$
t = 60h
OL - II
OL - I
SUBSCALE
UNREACTED ALLOY
I′
I″
IRON
SULFUR
NICKEL
CHROMIUM
COMPOSITION (WEIGHT %)
DISTANCE, μm
0
20
40
60
100
200
300
400
500
600

Fig. 12

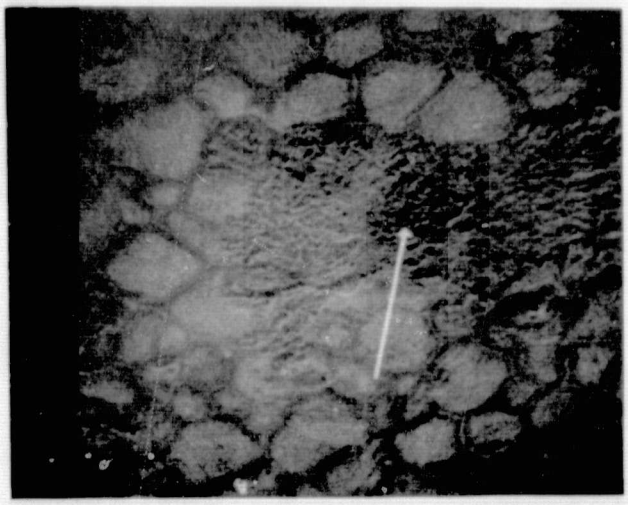

Fig. 13

ORIGINAL PAGE IS
OF POOR QUALITY

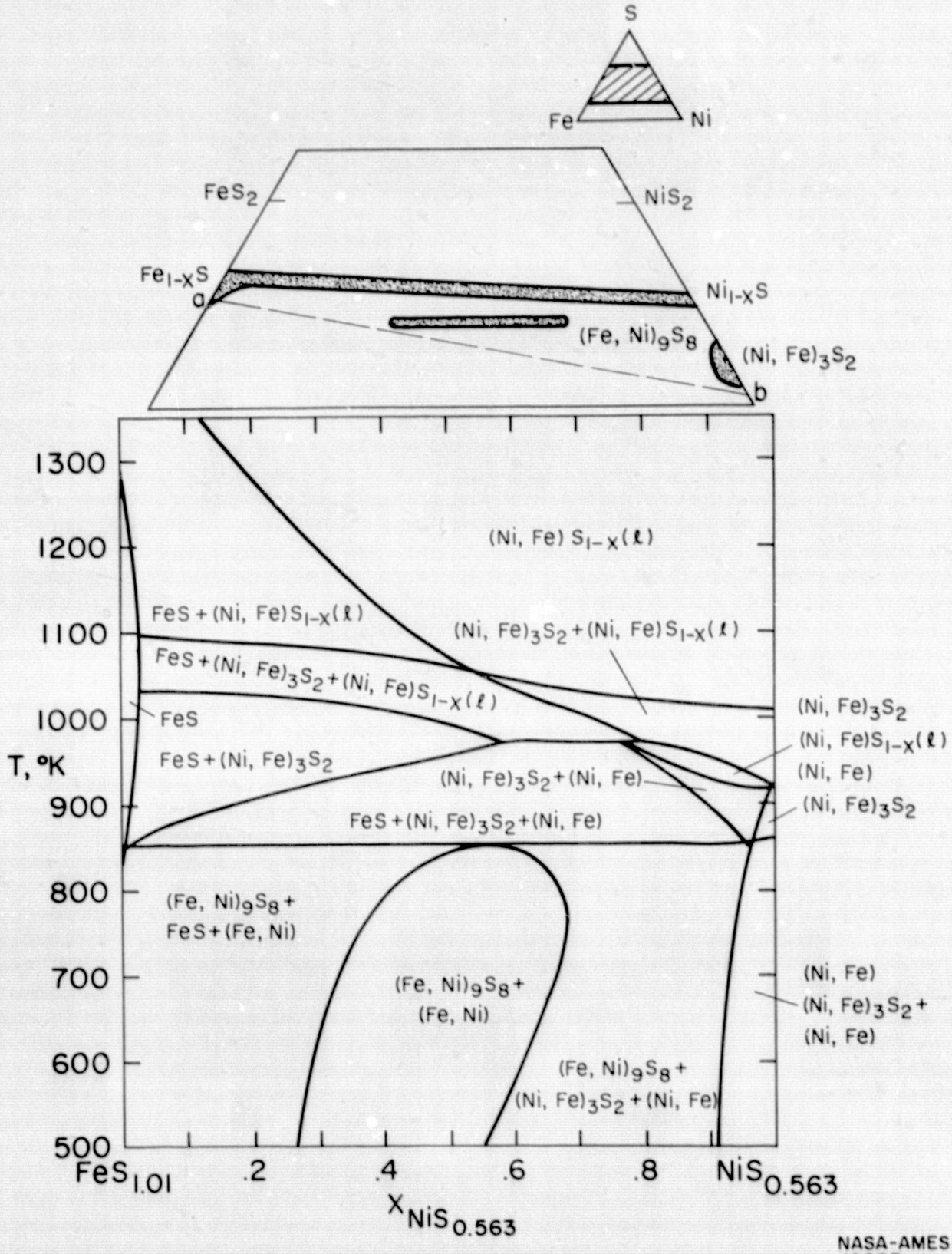

NASA-AMES
JACOB

Fig. 14

1. Report No.	2. Government Accession No.	3. Recipient's Catalog No.
NASA TM-78,465		

4. Title and Subtitle	5. Report Date
OF PHASE RELATIONS IN THE Fe-Ni-Cr-S SYSTEM AND THE SULFIDATION OF AN AUSTINITIC STAINLESS STEEL	6. Performing Organization Code
7. Author(s) K. T. Jacob,* D. Bhogeswara Rao,** and Howard G. Nelson	8. Performing Organization Report No. A-7309
9. Performing Organization Name and Address *University of California, Berkeley, CA 94720, **Lawrence Berkeley Laboratory, Berkeley, CA 94720, and NASA Ames Research Center, Moffett Field, CA 94035	10. Work Unit No. 505-01-21
	11. Contract or Grant No.
12. Sponsoring Agency Name and Address National Aeronautics and Space Administration, Wasington, D. C. 20546	13. Type of Report and Period Covered Technical Memorandum
	14. Sponsoring Agency Code

15. Supplementary Notes

16. Abstract

The stability fields of various sulfide phases that form on Fe-Cr, Fe-Ni, Ni-Cr and Fe-Cr-Ni alloys have been developed as a function of temperature and the partial pressure of sulfur. The calculated stability fields in the ternary A-B-S system are displayed on plots of log P_{S_2} versus the conjugate extensive variable (n_A/n_A+n_B), which provides a better framework for following the sulfidation of Fe-Cr-Ni alloys at high temperatures. Experimental and estimated thermodynamic data were used in developing the sulfur potential diagrams. Current models and correlations were employed to estimate the unknown thermodynamic behavior of solid solutions of sulfides and to supplement the income phase diagram data of geophysical literature. These constructed stability field diagrams are in excellent agreement with the sulfide phases and compositions determined experimentally during the sulfidation of SAE 310 stainless steel. The sulfur potential polots appear to be very useful in predicting and correlating the sulfidation of commercial alloys.

17. Key Words (Suggested by Author(s))	18. Distribution Statement
Thermochemical Diagrams Fe-Cr-S System Fe-Ni-S System Ni-Cr-S System Fe-Ni-Cr-S System	Unlimited STAR Category - 23

19. Security Classif. (of this report)	20. Security Classif. (of this page)	21. No. of Pages	22. Price*
Unclassified	Unclassified	59	$4.50

*For sale by the National Technical Information Service, Springfield, Virginia 22161